Plant Communications, Volume *1*

Supplemental Information

Integrative Multi-omics Analyses of Barley Rootzones under Salinity Stress Reveal Two Distinctive Salt Tolerance Mechanisms

William Wing Ho Ho, Camilla B. Hill, Monika S. Doblin, Megan C. Shelden, Allison van de Meene, Thusitha Rupasinghe, Antony Bacic, and Ute Roessner

Supplemental Information

Resource Article: Integrative Multi-Omics Analyses of Barley Rootzones Under Salinity Stress Reveal Two Distinctive Salt Tolerance Mechanisms

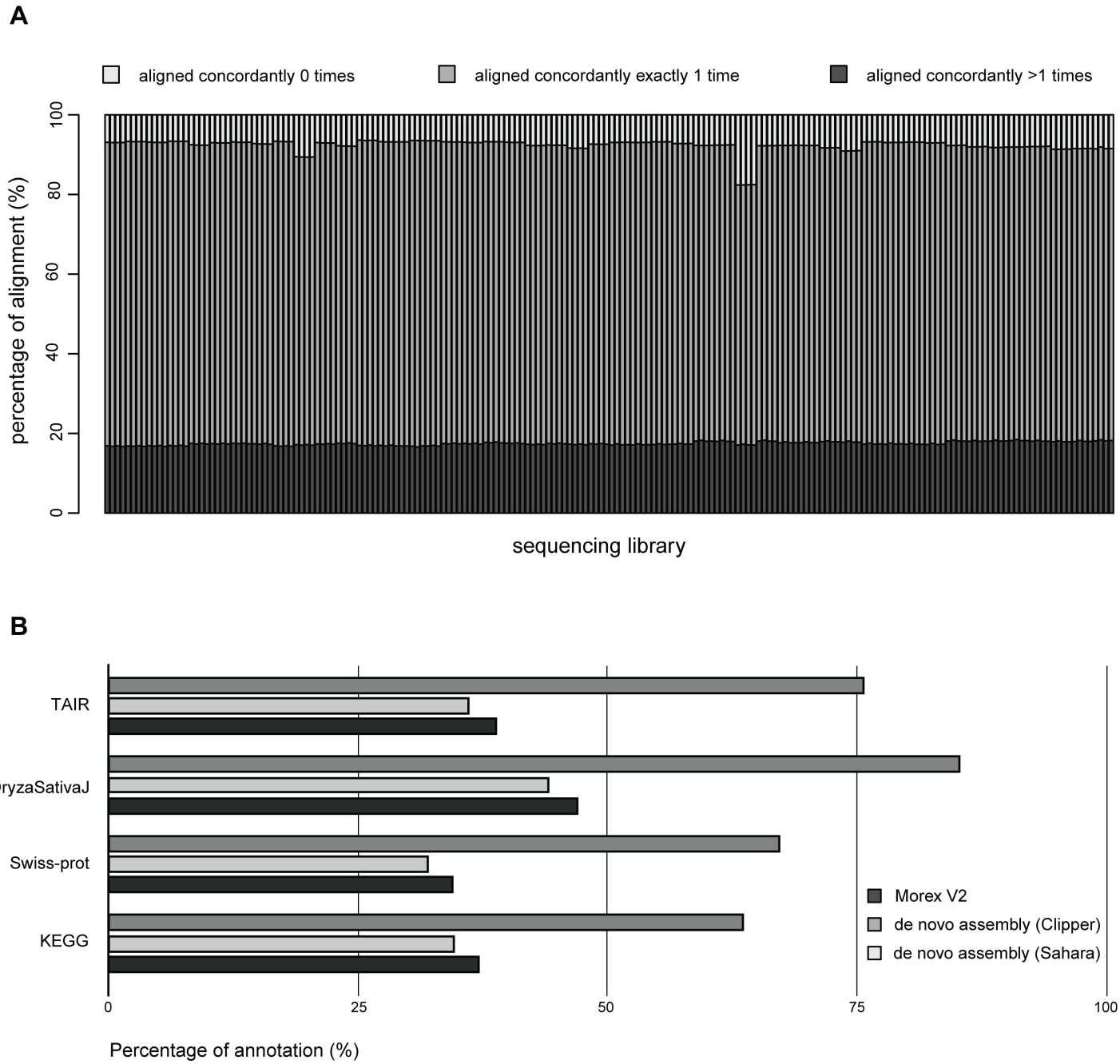

Supplemental Figure 1. Overview for mapping and functional annotation of different barley genomes or assemblies.

(A) Mapping efficiency of the 192 RNA-seq libraries. Each stacked bar represents the rate of alignment for each technical sequencing replicate per biological sample. Average of the overall alignment rate across the 192 sequencing libraries is 95.71 ± 1.60 %.

(B) Degree of functional annotation of the latest version of barley genome (cv. Morex), and of the *de novo* Assemblies (cv. Clipper and landrace Sahara) against the four major databases of functional annotations. The four representative functional annotation databases are TAIR (Arabidopsis thaliana: model dicot), RAP-DB (Oryza sativa cv. japonica: model monocot), Swiss-Prot (manually curated protein databank across organisms), and KEGG (molecular pathway database across organisms) are used in the comparisons. Average percentage of functional annotations for Morex V2, de novo assembly for Clipper and Sahara are 74.05%, 37.39%, and 40.06%, respectively. Only matches with E-value <1.00E-4 against the databases are considered as positively annotated.

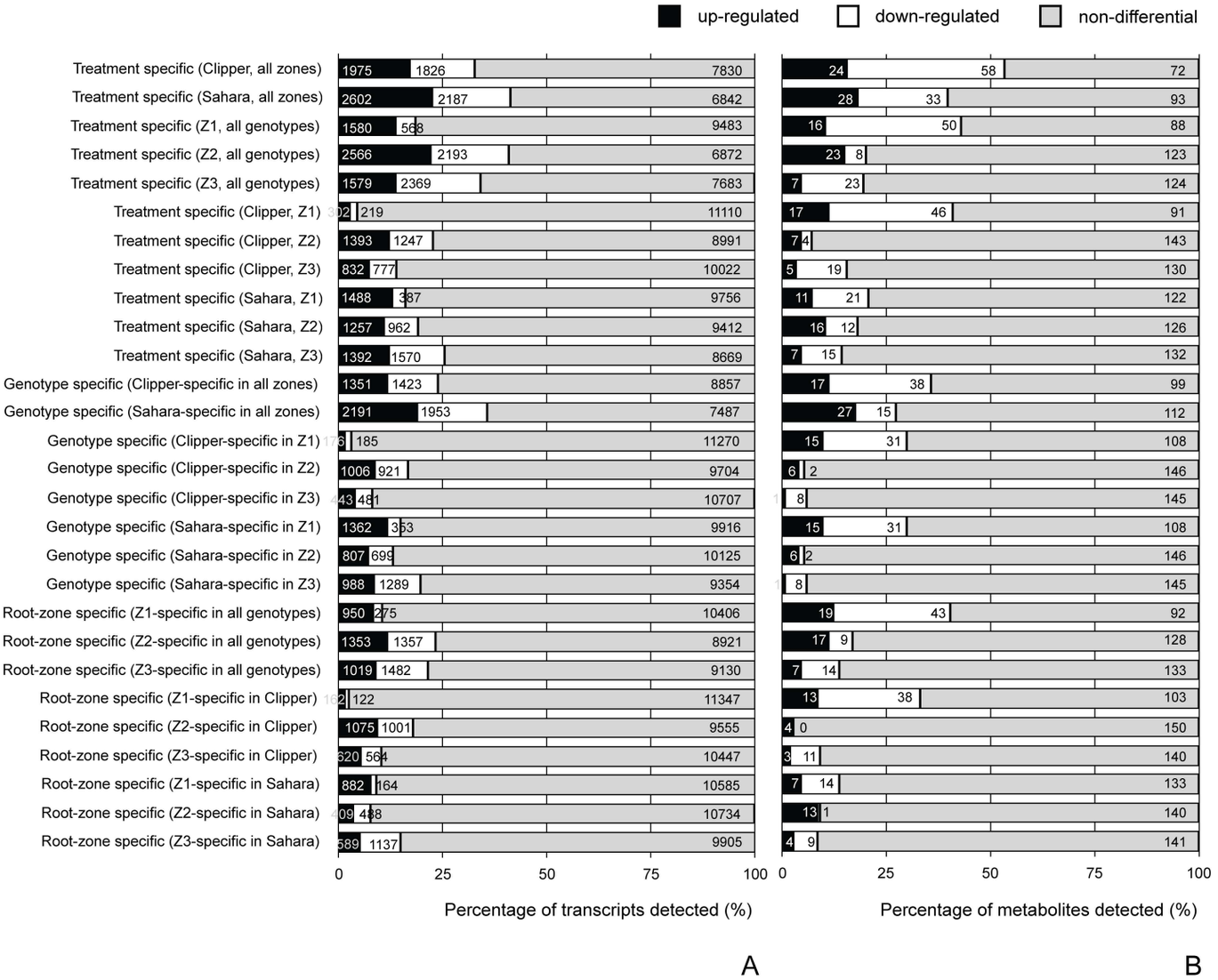

Supplemental Figure 2. Overview of the treatment-specific, genotype-specific, and rootzone-specific DEG and DAM of the two barley genotypes upon salt stress.

(A) Percentage of DEG and non-DEG with respect to the two treatments, two genotypes, and three rootzones. According to the latest version of the reference genome of barley (Mascher et al, 2017), cultivar Morex was predicted to have 85,493 of potential transcripts. However, only 11,631 transcripts were shown to have a minimal counts-per-million-reads of 10 in at least four replicates of our datasets among the predicted pool of transcripts in response to salt stress. Among the 11,631 detected transcripts, the GLM-based differential analyses revealed that the abundance of 3,801 transcripts (32.7%) changed significantly (up- or down-regulated) after the salt treatment in Clipper. In Sahara, 4,789 transcripts (41.2%) were significantly different in abundance in response to salt treatment relative to their controls, indicating the overall change in gene expression induced by salt was more pronounced in Sahara than in Clipper. From the perspective of rootzones within both barley genotypes, 2,148 (18.5%), 4,759 (40.9%), and 3,948 (33.9%) transcripts within the 11,631 quantifiable pool altered significantly after the salt treatment in Z1, Z2, and Z3, respectively. This suggests that the effect of salinity was more substantial in Z2, followed by Z3 and then Z1 at the transcript level in both genotypes. Further, among the 3,801 treatment-specific DEG in Clipper, 2,774 transcripts (73.0%) were shown to be highly specific to their genotype, compared to 4,144 (86.5%) transcripts within the 4,789 treatment-specific DEG in Sahara. In contrast, among the treatment-specific DEG in Z1 (2,148), Z2 (4,759), and Z3 (3,948), only 1,225 (57.0%), 2,710 (56.9%), and 1,501 (38.0%) transcripts were found to be highly specific to their respective rootzones. This indicates the salt-induced responses at transcript level in roots were more dependent on their genotypes than on their developmental zones.

(B) Percentage of DAM and non-DAM with respect to the two treatments, two genotypes, and three rootzones. In our experiment, 154 metabolites are within the limit of quantification of GC-QqQ-MS or LC-QqQ-MS after salt treatment. The GLM-based differential analyses showed that the abundance of 82 (53.3%) and 61 compounds (39.6%) varied significantly with salt treatment in both Clipper and Sahara relative to their controls, respectively. Across the root-zones, the abundance of 66 (42.9%), 31 (20.1%), and 30 (19.5%) compounds among the 154 quantifiable pools of metabolites changed significantly after the salt treatment in Z1, Z2, and Z3 of both genotypes, respectively. Furthermore, within the 82 treatment-specific DAM in Clipper, 55 compounds (67.1%) were shown to be highly specific to this genotype, compared to 42 compounds (68.9%) among the 61 treatment-specific DAM in Sahara. In comparison, among the treatment-specific DAM in Z1 (66 compounds), Z2 (31 compounds), and Z3 (30 compounds), 62 (93.9%), 26 (83.8%), and 21 (70.0%) compounds were found to be highly specific to their respective rootzones. The differential analyses at the primary metabolite and lipid levels suggest a higher degree of dependence of the salt-induced responses on root-zones than on genotype, compared to the transcriptional level. This implies an intriguing dynamic, where gene expression differences due to salt treatment are dominated by genotype and the downstream metabolic outcome is more influenced by rootzones.

Statistically significant differential gene expression or metabolite abundance is defined at a cutoff of FDR-adjusted p-value ≤ 0.05. Up- or down-regulation is defined by expression or abundance level relative to the corresponding uninduced control. Numbering at each segment of stacked bar of (A) and (B) represents the corresponding number of transcripts detectable by RNAseq and of metabolites detectable by GC-QqQ-MS and LC-QqQ-MS, respectively. DAM, differentially abundant metabolites; DEG, differentially expressed genes; Z1, zone 1 (meristematic zone); Z2, zone 2 (elongation zone); Z3, zone 3 (maturation zone).

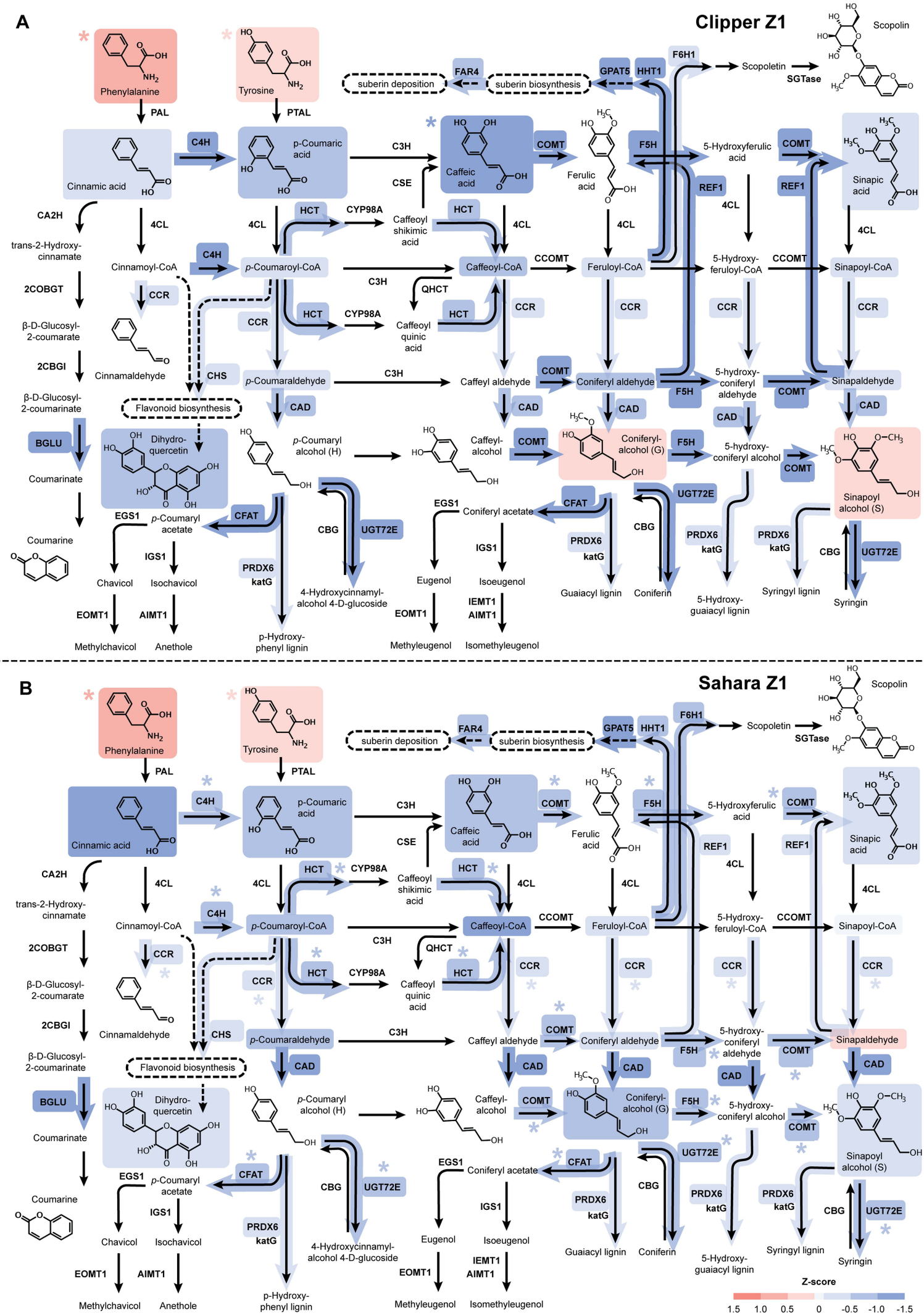

Supplemental Figure 3. Levels of transcripts and metabolites involved in phenylpropanoid biosynthesis at Z1 of the two barley genotypes under salt stress.

(A) The abundance of transcripts and metabolites involved in the biosynthesis at Clipper Z1.
(B) The abundance of transcripts and metabolites involved in the biosynthesis at Sahara Z1.

Values, color code, and full names for products of transcripts are given in **Figure 5**.

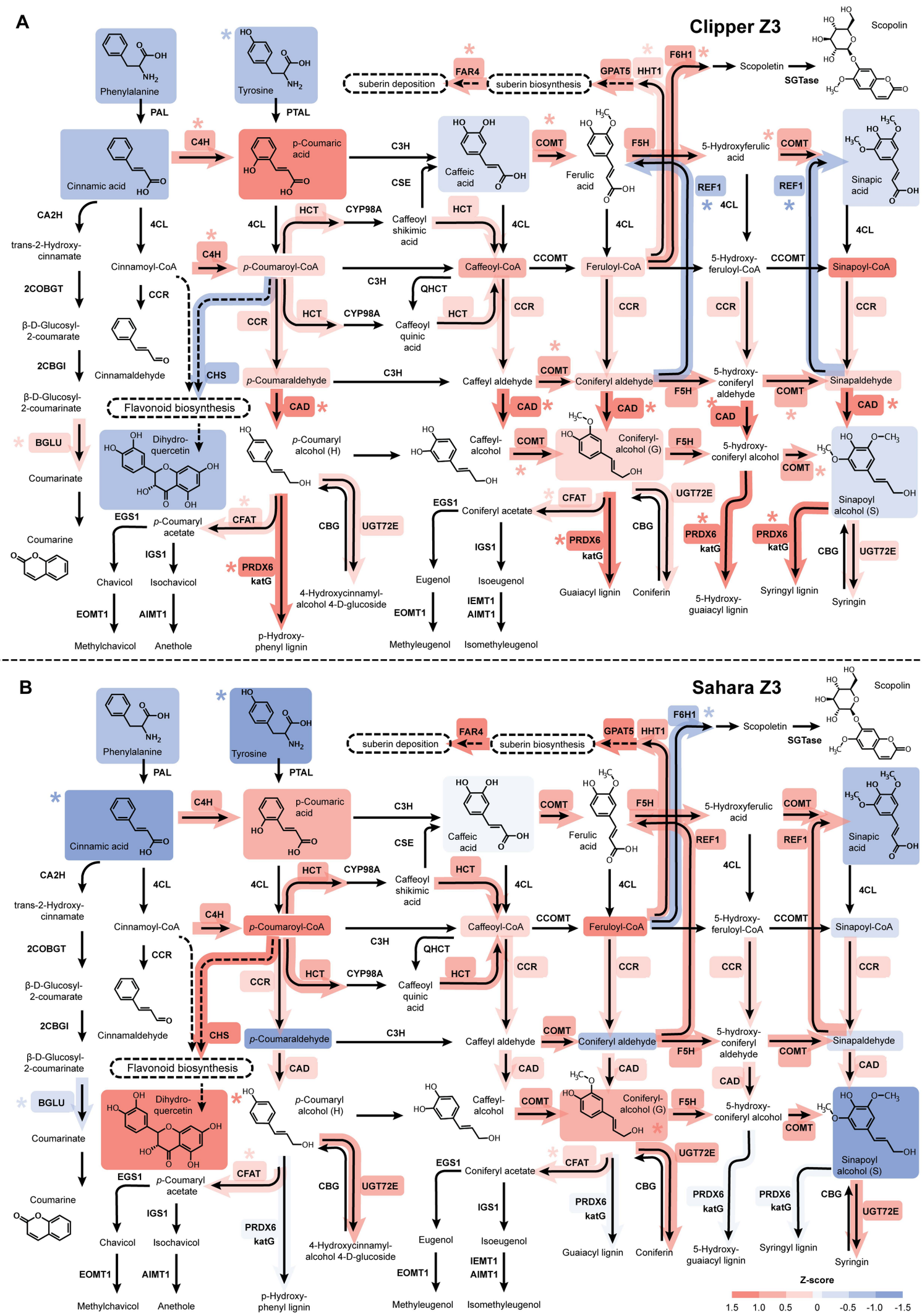

Supplemental Figure 4. Levels of transcripts and metabolites involved in phenylpropanoid biosynthesis at Z3 of the two barley genotypes under salt stress.

(A) The abundance of transcripts and metabolites involved in the biosynthesis at Clipper Z3.
(B) The abundance of transcripts and metabolites involved in the biosynthesis at Sahara Z3.

Values, color code, and full names for products of transcripts are given in **Figure 5**.

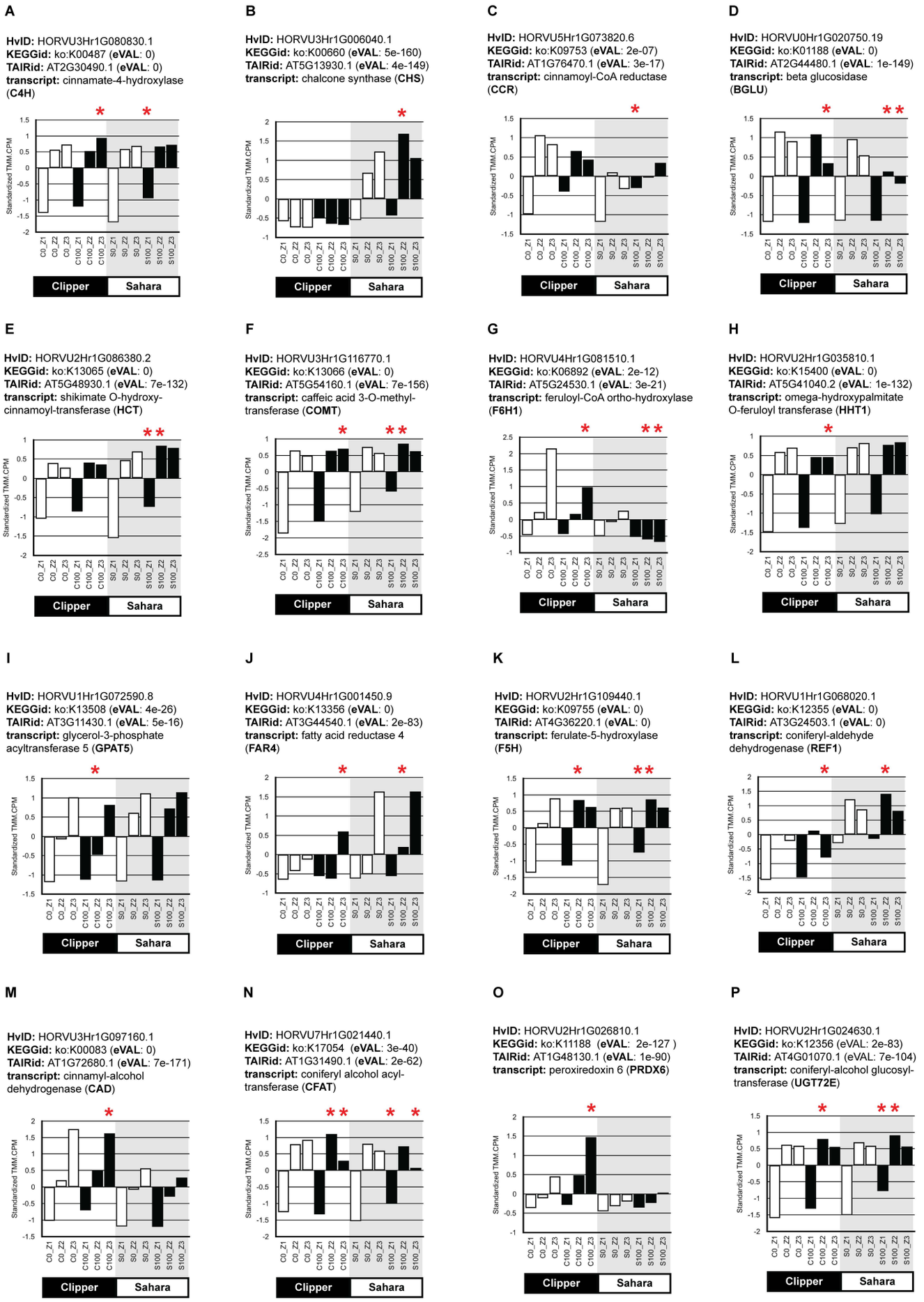

Supplemental Figure 5. Standardized abundance of transcripts involved in phenylpropanoid biosynthesis in Clipper and/or Sahara in response to salt stress.

Standardized abundances of transcripts are calculated by generating the Z-score for TMM normalized CPM. Statistically significant differentiation (with Benjamini-Hochberg adjusted *p* value < 0.05) of transcript-abundance upon salt treatment are indicated by red asterisks.

C0, Clipper treated with 0mM NaCl; C100, Clipper treated with 100mM NaCl; eVAL, E-value (for the corresponding BLAST search); HvID, ID of transcripts based on the deep-sequenced genome of *Hordeum vulgare* L. (cv. Morex) (Mascher et al., 2017.); KEGGid, identifiers of Kyoto Encyclopedia of Genes and Genomes database; S0, Sahara treated with 0mM NaCl; S100, Sahara treated with 100mM NaCl; TAIRid, identifier of The Arabidopsis Information Resource; TMM.CPM, trimmed mean of M-values normalized count per millions reads; Z1, meristemic zone (zone 1); Z2, elongation zone (zone 2); Z3, maturation zone.

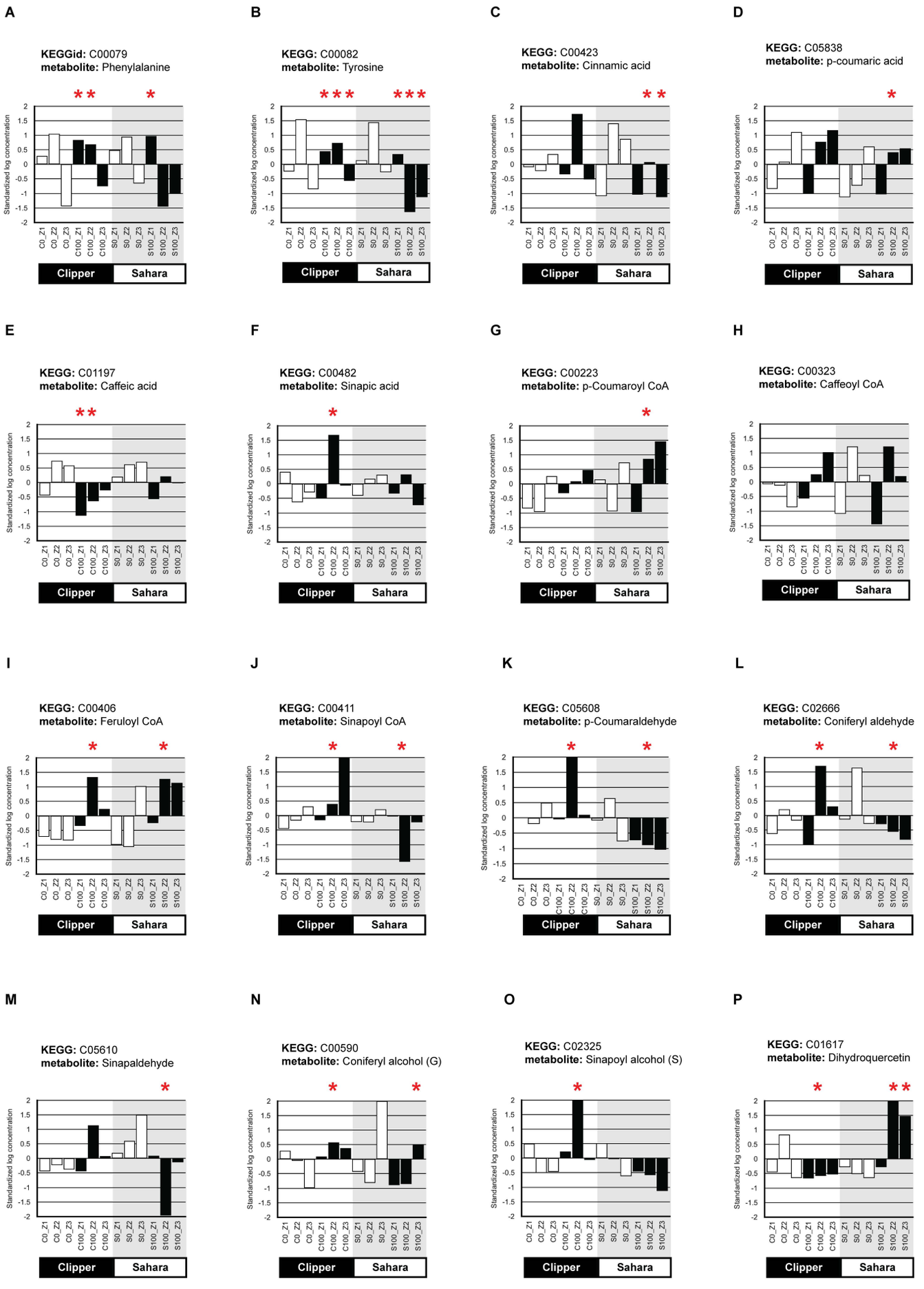

Supplemental Figure 6. Standardized abundance of metabolites involved in phenylpropanoid biosynthesis in Clipper and/or Sahara in response to salt stress.

Standardized abundances of metabolites are calculated by generating the Z-score for the median-normalized concentration. Statistically significant differentiation (with Benjamini-Hochberg adjusted p value < 0.05) of metabolite-abundance upon salt treatment are indicated by red asterisks. C0, Clipper treated with 0mM NaCl; C100, Clipper treated with 100mM NaCl; eVAL, E-value (for the corresponding BLAST search); KEGGid, identifiers of Kyoto Encyclopedia of Genes and Genomes database; S0, Sahara treated with 0mM NaCl; S100, Sahara treated with 100mM NaCl; Z1, meristemic zone (zone 1); Z2, elongation zone (zone 2); Z3, maturation zone.

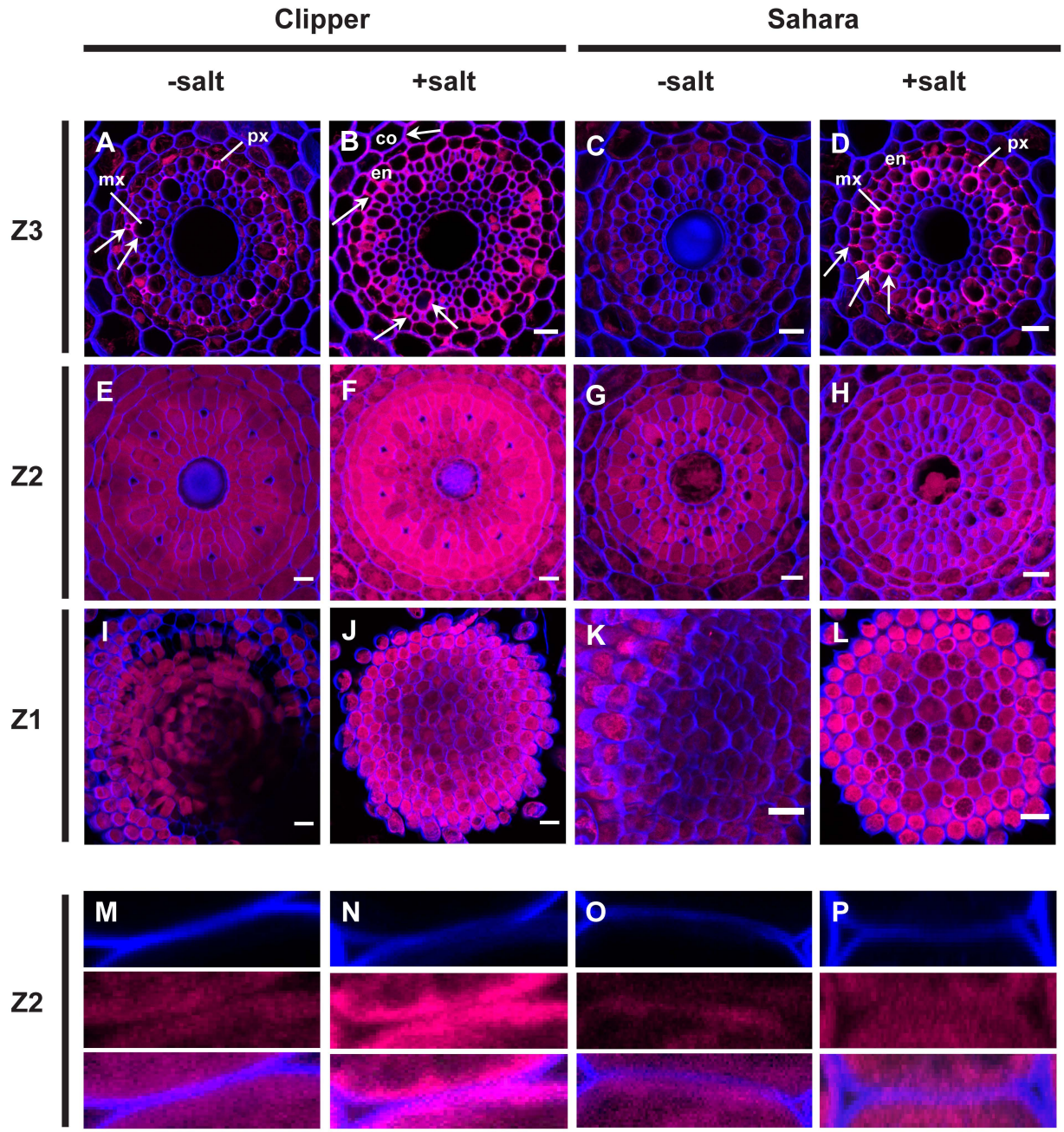

Supplemental Figure 7. Salinity-induced abundance and localization shift of lignin between different rootzones of the two barley genotypes upon salt stress.

Transverse sections from different rootzones of the two genotypes grown under 0mM NaCl (Clipper: **A,E,I,M**; Sahara: **C,G,K,O**) or 100mM NaCl (Clipper: **B,F,J,N**; Sahara: **D,H,L,P**) observed using confocal microscopy with the fluorescent lignin stain Basic Fuschin (magenta) and the general cell wall stain Calcofluor White (blue). **M,N,O,P** are the magnified views (upper panel: Calcofluor White stain only; middle panel: Basic Fuschin fluorescent stain only; lower panel: overlay of the two images) to the cell walls of endodermal cells at Z2 of Clipper (-salt), Clipper (+salt), Sahara (-salt), and Sahara (+salt), respectively.

Basic Fuschin interacts with lignin but also acidic components of the cytoplasm. Lignin presence was expected when the blue and magenta signals overlapped, but not in the cytoplasm of cells. Wall lignin was most obvious in Z3 (**A-D**). While tiny amount of lignin (white arrows) is detected in xylem vessels of Clipper with no salt treatment (**A**), a remarkable amount of lignin is deposited around the proto- and meta-xylem (**px** and **mx** respectively) and in the walls of the endodermal (**en**) and cortical (**co**) cells after salt treatment (**B**). For Sahara, very little lignin was observed in Z3 of the non-salt treated roots (**C**); however, intense deposits of lignin were observed in the meta- and proto-xylemic cell walls, accompanied by a small amount of lignins laid at walls of endodermis and pericycle after salt treatment (**D**). In Z2, most of the outer stelic layers including endodermal, periclinal, and xylemic regions of Clipper Z2 show a much higher intensity of magenta (**F**) than Sahara Z2 after the salt treatment (**H**). Compared to the magnified view to the endodermal cells of Sahara Z2 (**P**), the view at Clipper Z2 also shows a more intense magenta fluorescence at cell walls (indicated by the blue fluorescence) rather than in cytoplasm (**N**), suggesting the increased lignin deposition occurred at cell walls of Clipper Z2, but not of Sahara Z2. Scale bars = 50 μm (**A, C, E, G, L, K, M, O, Q, S, U , W**) or 20 μm (**B, D, F, H, J, L, N, P, R, T, V, X**).

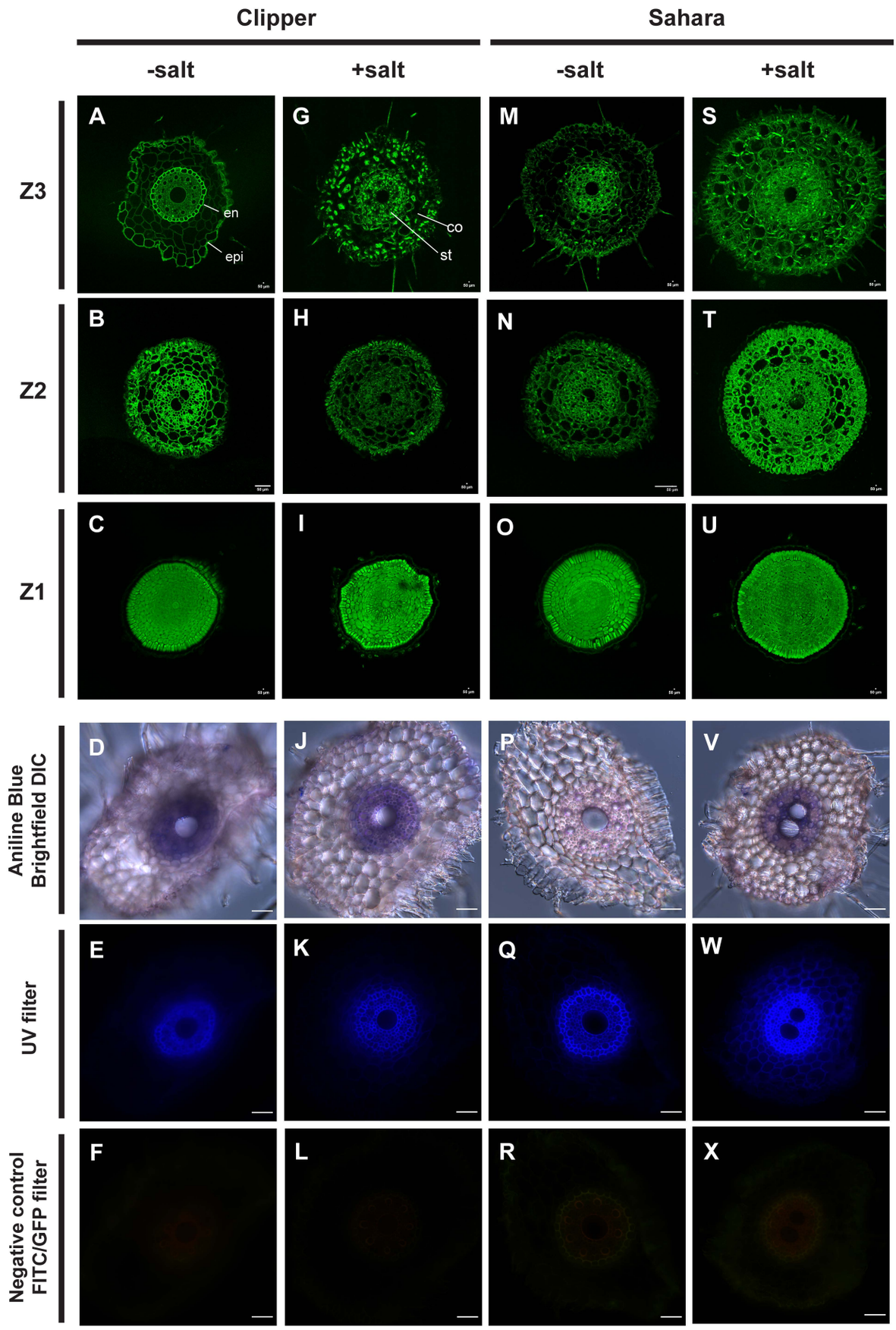

Supplemental Figure 8. Salinity-induced abundance and localization shift of suberin between different rootzones of the two barley genotypes upon salt stress.

Transverse sections from different rootzones of the two genotypes grown under 0mM NaCl (Clipper: **A-F**; Sahara: **M-R**) or 100mM NaCl (Clipper: **G-L**; Sahara: **S-X**) using confocal microscopy with Fluorol Yellow, a fluorescent suberin-specific stain, observed under FITC/GFP filter (Clipper: **A-C,G-I**; Sahara: **M-O,S-U**), or Z3 root sections (Clipper: **D-F,P-R**; Sahara: **J-L,V-X**) without staining with Fluorol Yellow observed under brightfield DIC (**D,J,P,V**), UV filter (**E,K,Q,W**), or FITC/GFP filter (**F,L,R,X**). Fluorol Yellow is a suberin-specific stain. The Aniline Blue (**D,J,P,V**) is a counterstain, which show the cytoplasmic details and structure in roots under brightfield DIC. The UV filter (**E,K,Q,W**) shows autofluorescence from lignin and other wall components such as vasculature. The negative control (**F,L,R,X**) underwent the same treatment except staining with Fluorol Yellow. Only a minimal autofluorescence can be observed under the FITC/GFP filter. Scale bars = 50µm. co, cortex; DIC, differential interference contrast; en, endodermis; epi, epidermis; FITC, fluorescein isothiocyanate; GFP, green fluorescent protein; st, stele; UV, ultraviolet.

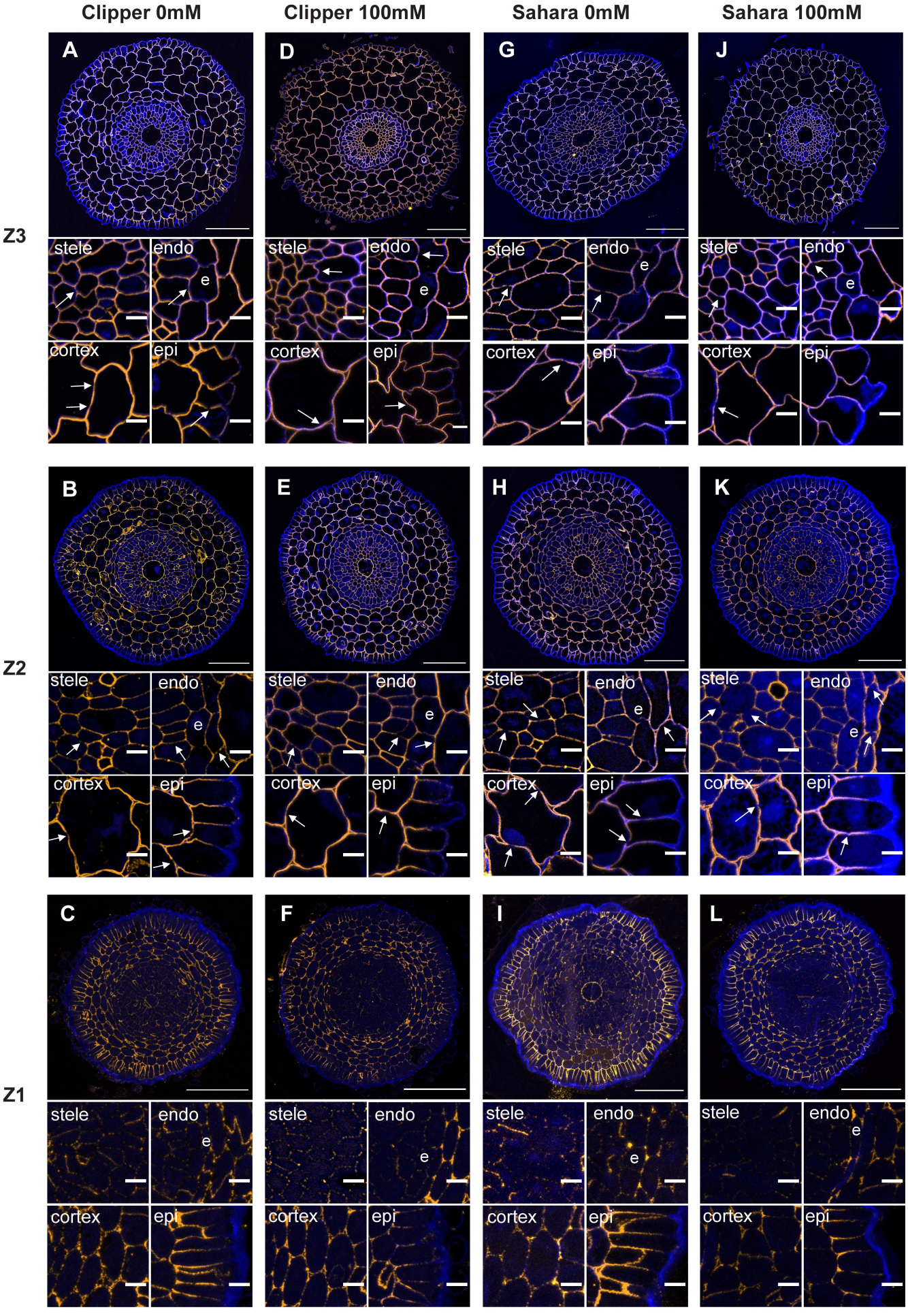

Supplemental Figure 9. Salinity-induced abundance and localization shift of callose between different rootzones of the two barley genotypes upon salt stress.

Transverse sections from different rootzones of the two genotypes grown under 0mM NaCl (Clipper: A-C; Sahara: G-I) or 100mM NaCl (Clipper: D-F; Sahara: J-L) observed using confocal microscopy for the callose (anti-(1,3)-beta-glucan) antibodies (orange) and autofluorescence (blue). From each genotype, rootzone, and treatment, higher magnification images of cells at the central stele (stele), endodermis (endo; endodermal layer is denoted by 'e'), cortical cells (cortex) or epidermis (epi) are shown below each transverse section. Plasmodesmata are present in some cells (arrows). In Z1, callose is deposited in a punctate pattern and plasmodesmata are not obvious. Scale bars = 100 µm (for whole sections); 10 µm (for magnified cell images).

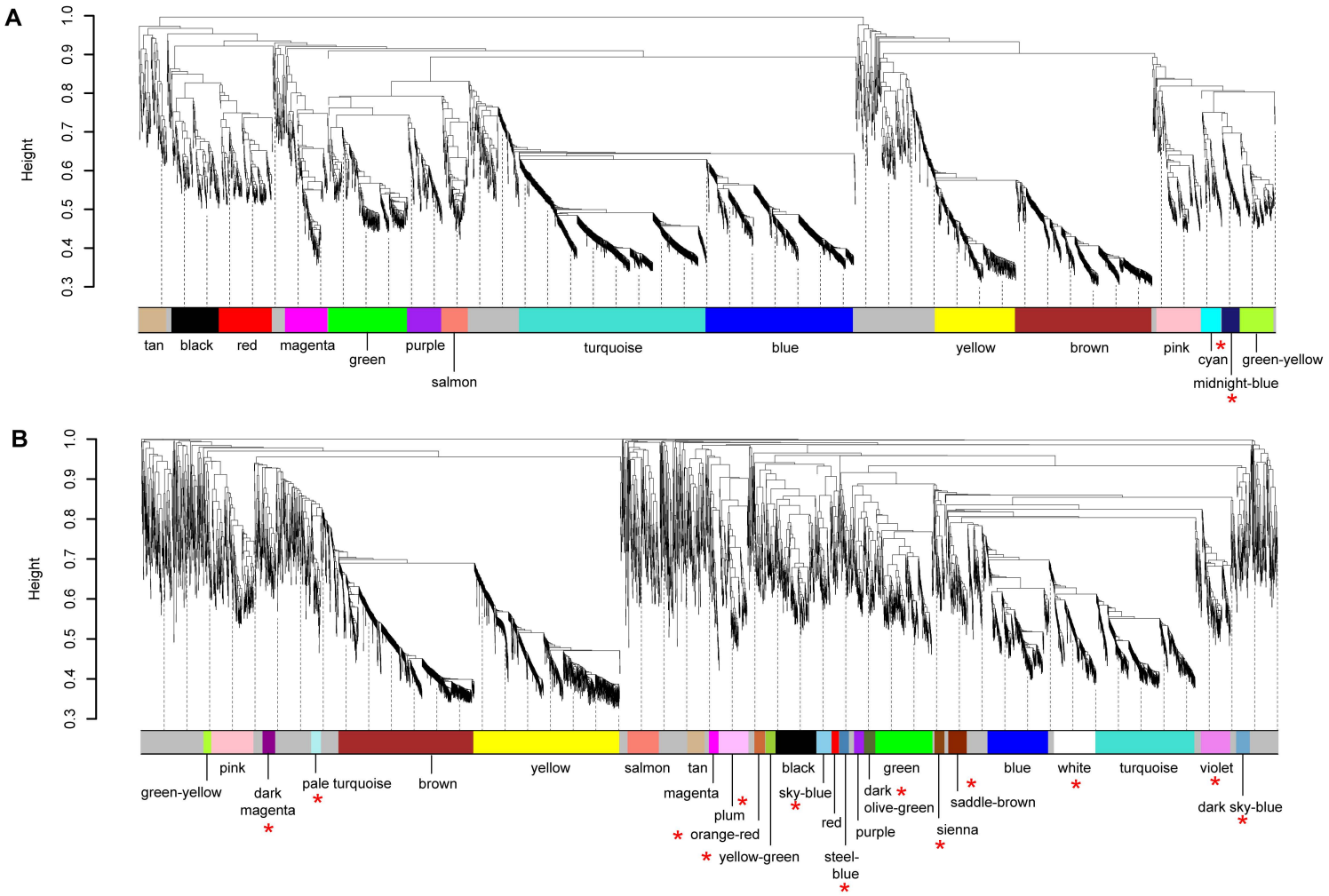

Supplemental Figure 10. Clustering dendrograms of global gene-coexpression in each barley genotype with dissimilarity based on topological overlap.

(A) Global gene-coexpression clustering of Hordeum vulgare L. cv. Clipper. Sixteen different module-colors are assigned for each coexpression cluster, which include: turquoise, blue, tan, green, grey, black, brown, yellow, magenta, red, purple, cyan, midnight-blue, salmon, pink, and greenyellow.

(B) Global gene-coexpression clustering of the landrace Sahara. Twenty-seven different module-colors are assigned for each coexpression cluster, which include: turquoise, blue, white, yellow, green, orange-red, sienna, grey, yellow-green, tan, brown, salmon, dark-magenta, red, plum, black, pink, saddlebrown, violet, pale-turquoise, dark-olivegreen, skyblue, magenta, dark skyblue, purple, greenyellow, and steel-blue.

Red asterisks beneath each assigned module-color indicate modules unique to Clipper or to Sahara. Grey-colored modules representing genes with unclustered expression pattern are not labelled for clarity.

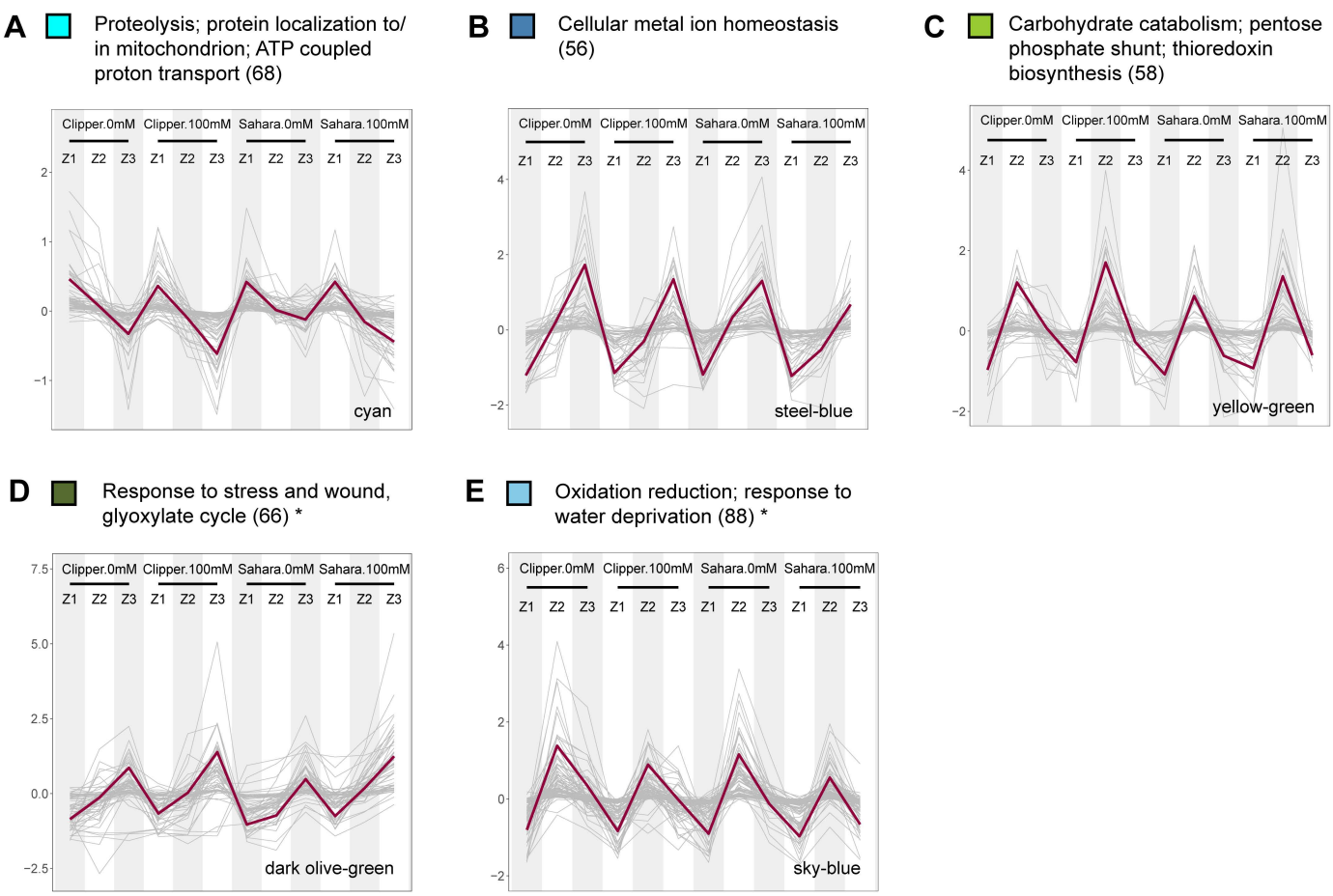

Supplemental Figure 11. Additional modules of weighted coexpression correlation networks showing abundance profiles of transcripts and metabolites unique to either Clipper or Sahara.

(A) The abundance profile unique to Clipper or significantly contrast from Sahara.
(B-E) The abundance profiles unique to Sahara or significantly contrast from Clipper.

These modules are considered as additional or minor due to their non-apparent difference of profiles between Clipper and Sahara. Annotated lists of members for each module with signficant match (E-value < 1.00E-4) against TAIR10 genome release (version: Jun 2016) ranked in descending order according to kME of members can be found in **Supplemental Data Set 9 online**. For abbreviations and symbols, see **Figure 6**.

Supplemental Note 1

To derive the genotype-specific DEG for each root zone, we first clustered the twelve transcriptomes into four groups based on genotype (Clipper, C; Sahara, S) and treatment (untreated, U; treated, T).

Genotype	Treatment	Group
Clipper	salt-treated	CT
Clipper	untreated	CU
Sahara	salt-treated	ST
Sahara	untreated	SU

Second, DEG upon salt treatment in a genotype were determined by fitting basic GLM to test for the "contrasts" (a term for describing GLM-based comparisons as defined by (Chen et al.) and was denoted as " < > " in this work) between the treated and untreated pairs: CT < > CU and ST < > SU. For each "contrast", we designated genes that were significantly different (adjusted *p* value <0.05) in Clipper as sector A and in Sahara as sector B (Figure 2C). Third, to find DEG due to salt treatment between Clipper and Sahara, we fitted interaction GLM considering the interactions between genotypes and treatments to form "contrasts": (CT < > CU) < > (ST < > SU) and (ST < > SU) < > (CT < > CU). Genes expressed significantly differently (adjusted *p* value <0.05) between the genotypes were defined within sector C (Figure 2C). Fourth, we intersected the three sectors. Subsector A - (C ∪ B) corresponded to DEG unique to Clipper, subsector A ∩ B ∩ C corresponded to DEG significantly different in expression between the two genotypes, and subsector (A ∩ C) - B corresponded to DEG unique to Clipper and significantly differed between the two genotypes at the same time, which three subsectors together constituted the Clipper-specific DEG in a root zone. Accordingly, subsectors B - (A ∪ C), A ∩ B ∩ C, and (B ∩ C) - A represented the Sahara-specific DEG for each root zone (Figure 2C).

To derive the root zone-specific DEG for each genotype, similar to the derivation of the genotype-specific DEG, we clustered the twelve transcriptomes into six groups, namely salt-treated Z1 (group Z1T), untreated Z1 (group Z1U), salt-treated Z2 (group Z2T), untreated Z2 (group Z2U), salt-treated Z3 (group Z3T), and untreated Z3 (group Z3U).

Root-zone	**Treatment**	**Group**
Z1	salt-treated	Z1T
Z1	untreated	Z1U
Z2	salt-treated	Z2T
Z2	untreated	Z2U
Z3	salt-treated	Z3T
Z3	untreated	Z3U

Second, to find DEG upon salt treatment for each root zone, we fitted basic GLM to form "contrasts" between the treated and untreated pairs, including Z1T < > Z1U (for Z1), Z2T < > Z2U (for Z2) and Z3T < > Z3U (for Z3). Genes expressed significantly different (adjusted *p* value <0.05) in Z1, Z2, and Z3 were designated as sector D, E, and F, respectively (Figure 2D to 2F). Third, to find DEG responded differently to salt among the three root zones, we used interaction GLM considering the interactions between root zones and treatments to form "contrasts": (Z2T < > Z2U) < > (Z1T < > Z1U), and (Z3T < > Z3U) < > (Z1T < > Z1U) (for Z1 meristematic zone); (Z1T < > Z1U) < > (Z2T < > Z2U), and (Z3T < > Z3U) < > (Z2T < > Z2U) (for Z2 elongation zone); (Z1T < > Z1U) < > (Z3T < > Z3U), and (Z2T < > Z2U) < > (Z3T < > Z3U) (for Z3 maturation zone). For each "contrast", we selected genes that were significantly different (adjusted *p* value <0.05) as sector G, H, I, J, K, and L, respectively (Figure 2D to 2F). Fourth, we intersected the five sectors in each root zone. Subsectors D - (E ∪ F ∪ G ∪ H), (D ∩ G) - (E ∪ F ∪ H), and (D ∩ H) - (E ∪ F ∪ G) correspond to DEG unique to Z1; subsectors D ∩ E ∩ F ∩ G ∩ H, (D ∩ E ∩ G ∩ H) - F, (D ∩ F ∩ G ∩ H) - E corresponds to DEG with expression at Z1 significantly different from the other two root zones; subsector (D ∩ G ∩ H) - E ∪ F corresponds to DEG unique to Z1 and as well as significantly differential from Z2 and Z3 at the same time, which five subsectors together constituted the Z1-specific DEG for each genotype (Figure 2D). Accordingly, subsectors E - (D ∪ F ∪ I ∪ J), (D ∩ I) - (E

∪ F ∪ J), (E ∩ J) - (D ∪ F ∪ I); D ∩ E ∩ F ∩ I ∩ J, (D ∩ E ∩ I ∩ J) - F, (E ∩ F ∩ I ∩ J) - D; and (E ∩ I ∩ J) - (D ∪ F) indicated the Z2-specific DEG in for each genotype (Figure 2E). Subsectors F - (D ∪ E ∪ K ∪ L), (F ∩ K) - (D ∪ E ∪ L), (F ∩ L) - (D ∪ E ∪ K); D ∩ E ∩ F ∩ K ∩ L, (D ∩ F ∩ K ∩ L) - E, (E ∩ F ∩ K ∩ L) - D; and (F ∩ K ∩ L) - (D ∪ E) represented the Z3-specific DEG for each genotype (Figure 2F; for the detailed DEG lists, see Supplementary Data Set 3 online).

REFERENCES

Chen, Y., McCarthy, D., Matthew, Robinson, M., and Smyth, G. K. edgeR: differential expression analysis of digital gene expression data - User's Guide (First Edition). Available online at: https://www.bioconductor.org/packages/devel/bioc/vignettes/edgeR/inst/doc/edgeRUsersGuide.pdf.

Supplemental Note 2

Outcomes of Global Co-expression Correlation Network Analysis

Among the selected clusters, module A, J, K, L grouped members with stronger increase in abundance at Z2 of Clipper than Sahara upon salt stress. In which, **Module A** harboured 48 DEG and GO analysis revealed the most relevant biological processes to be multidimensional cell growth (Fig. 7A). In line with the growth-sustaining phenotype of Clipper under high salt conditions, a homolog of CELLULASE 1 (CEL1) (HORVU0Hr1G020000.1), which is a key player involved in cell elongation with endo-1,4-beta-glucanase activity, was found to be the modular member with the highest kME and known function (Shani et al., 1997) (Supplementary Data Set 8 and 9: sheet 'midnight-blue'). **Module J** comprises 138 DEG and glycine as the only DAM in this cluster. Enrichment analysis revealed a significant overrepresentation of biological processes involved in amino acid metabolism, response to stimulus, and cell wall organization (Fig. 7J). Among the GO category of response to stimulus, a barley homolog of glutamine receptor 2.7 (GLR2.7) (HORVU7Hr1G031530.1), which is known to be a member of the ligand-gated ion channel subunit family mediating cellular calcium ion homeostasis in response to abiotic stress of *Arabidopsis thaliana*, was pinpointed in this module (Kim et al., 2001). Also, a homolog of the EXPANSIN B2 (EXPB2) (HORVU1Hr1G054240.2) was found at the top of the kME list for this cluster. Although the induced abundance of this EXPB2 homolog in Clipper Z2 could not surpass its level in Sahara Z2 after salt, this could be in line with the fact that the regulatory roles of the huge family of EXPANSIN and EXPANSIN-like proteins are not limited to cell elongation only (Lee et al., 2001). As recently indicated by a study on an EXPB homolog in wheat, the EXPB2 in this cluster could rather play a common role in the two genotypes for regulating the activity of root cell wall-bound peroxidase under the oxidative pressure induced by salt (Han et al., 2015) (Supplementary Data Set 8 and 9: sheet 'black'). **Module K** represented 80 DEG upon high salinity stress. Amino acid transport, protein ubiquitination, and toxin catabolism were determined as the most relevant biological processes to this module (Fig. 7K). Coherent with the proposed involvement of its modular members in transport of amino acids, a barley transcript (HORVU5Hr1G093090.2) with sequence identical to its homolog in *Arabidopsis thaliana* or in *Oryza sativa* (E-value < 1.00E-250), which encoded for a type of cationic amino acid- / polyamine-transporters known as AMINO ACID TRANSPORTER 1 (AAT1), was

ranked fifth on the kME list of module K (Frommer et al., 1995). Polyamine is a known group of compounds involved in the regulation of redox homeostasis during salt stress in plants (Saha et al., 2015; Shu et al., 2015). Besides, GLUTATHIONE S-TRANSFERASE TAU18 (GST U18), a member of the glutathione S-transferase family belonging to the GO category of toxin catabolism, was identified in this cluster and shown to have higher transcript abundance at Z2 when comparing Clipper to Sahara. Evidence to demonstrate the importance of GSTs for minimising the damages induced by oxidative stress *in planta* were previously described in (Cummins et al., 1999; Kampranis et al., 2000; Roxas et al., 1997) (Supplementary Data Set 8 and 9: sheet 'purple'). **Module L** grouped 156 DEG with biological processes significantly enriched in cell wall loosening, auxin homeostasis and lignin biosynthesis (Fig. 7L). This cluster harboured the exact matches (E-value < 1.00E-250) of *CELLULOSE SYNTHASE 1* (CESA1) and *CELLULOSE SYNTHASE 3* (CESA3) in barley (HORVU6Hr1G013670.30, HORVU0Hr1G002350.1), with CESA1 being identified as the member with the highest kME of this module. Together with CESA6, CESA1 and CESA3 were known to form a hexameric plasma membrane complex mediating cellulose biosynthesis in primary cell wall (Desprez et al., 2007). Also, three transcripts (HORVU4Hr1G072660.1, HORVU4Hr1G072580.1, HORVU5Hr1G119680.2) encoded for homologs of EXPANSIN A11 (EXPA11), one transcript (HORVU6Hr1G063180.1) for EXPANSIN B4 (EXPB4), and one transcript (HORVU1Hr1G051640.1) for EXPANSIN A7 (EXPA7) were co-regulated in this cluster. Abundance of all five *EXPANSIN* were induced by salt and reached levels higher in Z2 of Clipper than Sahara, except *EXPA7*. Notably, besides a barley homolog of a key enzyme involved in brassinosteroid biosynthesis known as DEETIOLATED2 (DET2) (HORVU3Hr1G085400.1) was co-regulated in this cluster (Fujioka et al., 1997), three transcripts (HORVU5Hr1G035980.1, HORVU6Hr1G075650.1, HORVU4Hr1G019380.1) encoded for homologs of the TEOSINTE-BRANCHED 1/CYCLOIDEA/PCF1 (TCP) transcription factor family, namely TCP8, TCP15, and TCP23, which have their family recently been proven to involve in regulation of salicylic acid (SA) biosynthesis in response to range of plant abiotic stress responses, could also be pinpointed in this module (Lei et al., 2017; Wang et al., 2015) (Supplementary Data Set 8 and 9: sheet 'red').

In response to the salt treatment, **Module N** was the only cluster built up from members showing mostly drastic changes in abundance at Z3 of both genotypes, with a majority of the changes higher in Clipper than in Sahara. This module consisted of putrescine as the only DAM in the cluster and 107 DEG that were significantly enriched in biological processes such as cell

wall loosening, lipid storage and catabolism (Fig. 7N). Apart from a homolog of XYLOGLUCAN ENDOTRANSGLUCOSYLASE/HYDROLASE 13 (XTH13) (HORVU2Hr1G101150.1) known to involve in cell wall organization and biogenesis was grouped in this module (Thompson and Fry, 2001), we found two barley transcripts (HORVU3Hr1G058700.1, HORVU5Hr1G056030.1) co-regulated in this cluster with sequence well-matched to their dicot homologs, DAD1-LIKE SEEDING ESTABLISHMENT-RELATED LIPASE (*DSEL*) (E-value = 3.00E-125) and OLEOSIN 1 (*OLE1*) (E-value = 1.00E-16), respectively. Intriguingly, DSEL was shown to possess acylglycerol lipase activity and inhibits the breakdown of storage oils in seedlings, while OLE1 was known to have oilbody biogenic properties and involve in seed oil body formation for lipid accumulation in response to freezing stress in *A. thaliana* (Shimada et al., 2008; Kim et al., 2011). Transcript abundance of both *DSEL* and *OLE1* increased more strongly when compared Z3 of Clipper to Sahara after the salt treatment. In comparison, five transcripts (HORVU3Hr1G105160.1, HORVU3Hr1G073120.1, HORVU3Hr1G105180.1, HORVU7Hr1G119360.1, and HORVU2Hr1G093690.1) with sequences homologous to three paralogs of *EXPANSIN* in *A. thaliana* (namely *EXPA2*, *EXPA13*, *EXPB2*) were identified in this cluster and their abundance were boosted at Z3 of both genotypes upon salt. Except *EXPA13*, the abundance of these EXPANSIN were higher in Z3 of Sahara than Clipper and are likely to play a role in the oxidative stress tolerance as in Sahara Z2 (Supplementary Data Set 8 and 9: sheet 'magenta').

The subnetwork, including modules B, G, O, and I, was the co-expression cluster with members showing substantial decline in abundance at Z3 of both genotypes. **Module B** represented 177 DEG significantly overrepresented in nitrile biosynthesis, glycosinolate catabolism, and defence response (Fig. 7B). While abundance of the two barley homologs of *FLAVIN-DEPENDENT MONOOXYGENASE 1* (*FMO1)* (HORVU5Hr1G086710, HORVU5Hr1G086770) that was known to be a crucial component involved in the plant-type hypersensitive response were decreased to comparable levels in the two genotypes after the salt treatment (Mishina and Zeier, 2006), transcript level of four mannose-binding lectin (MBL) superfamily proteins (HORVU5Hr1G009040.2, HORVU5Hr1G009040.6, HORVU5Hr1G009040.5, HORVU5Hr1G009100.1) were consistently lower in Z3 of Sahara relative to Clipper upon salt stress. One of the well-characterized members of the MBL protein family is MYROSINASE-BINDING PROTEIN 1 (MBP1) and its presence was proven to be essential for the formation of myrosinase isoenzymes, which were found to play a key role in glucosinolate hydrolysis upon wounding in *Brassica napus* (Eriksson et al., 2002; Angelino et

al., 2015). Notably, transcripts encoding for a barley homolog of C-REPEAT BINDING FACTOR 3 (CBF3) (HORVU5Hr1G080300.1) was also found to be co-regulated in this cluster with its expression substantially suppressed in Clipper Z2 and Z3, but mostly unaffected in Sahara. CBF3 was proven to be a negative regulator of gibberellin signalling pathway through promotion of DELLA accumulation and *GIBBERELLIN 2-OXIDASE 7* (*GA2OX7*) expression (Zhou et al., 2017) (Supplementary Data Set 8 and 9: sheet 'white'). **Module G** comprised of 125 DEG and GO analysis revealed the most relevant biological processes to this cluster were lipid catabolism, phenylpropanoid biosynthesis, and cell wall modification (Fig. 7G). Among the category of lipid catabolic process, two transcripts in this cluster (HORVU3Hr1G068280.1, HORVU1Hr1G055840.1) were shown to be members of alpha/beta-hydrolases superfamily, of which HORVU1Hr1G055840.1 shared a high degree of sequence similarity with DAD1-LIKE LIPASE 1 (DALL1) in *A.thaliana* (E-value: 1.00E-112). DALL1 was shown to be capable of hydrolyzing triacylglycerols, phosphatidylcholines as well as glycolipids, and shown to act redundantly in jasmonate biosynthesis after wounding or in response to salt (Ellinger and Kubigsteltig, 2010; Ruduś et al., 2014). Higher abundance of *DALL1* induced or remained at Z1 and Z3 of Sahara than Clipper could indicate a higher accumulation of jasmonate in Sahara in response to osmotic damages caused by salt (Supplementary Data Set 8 and 9: sheet 'violet'). **Module O** was a co-expression cluster harboured 49 DEG, of which their abundance in Clipper Z3 were remained higher when compared to Sahara even after the suppression by salt stress. Based on the enrichment analysis, nicotianamine biosynthesis and phloem transport are the most significantly overrepresented biological processes (Fig. 7O). Intriguingly, four barley transcripts (HORVU4Hr1G089750.2, HORVU6Hr1G090040.4, HORVU0Hr1G017720.1, HORVU6Hr1G090180.1) encode NICOTIANAMINE SYNTHASE 3 (NAS3) and three other transcripts (HORVU4Hr1G089870.1, HORVU6Hr1G032290.1, HORVU4Hr1G087390.1) were the homologs of NICOTIANAMINE SYNTHASE 4 (NAS4) in barley (Supplementary Data Set 8 and 9: sheet 'salmon'). Previous findings showed that NAS genes in *Triticum aestivum* L. encode for enzymes that convert S-adenosyl-L-methionine to nicotianamine, which is a non-protein amino acid involved in fundamental aspects of metal homeostasis and was shown to confer higher salt tolerance to bread wheat (Bonneau et al., 2016). **Module I** harboured 44 DEG and tryptophan as the only DAM in this cluster. The most relevant biological process to this cluster is tryptophan metabolism, fatty acid metabolism, abscisic acid (ABA) signalling, and salt overly sensitive (SOS) pathway (Fig. 7I). While the abundance of barley transcripts (HORVU7Hr1G083490.7, HORVU2Hr1G117610.1) encoded for ACYL-CoA OXIDASE 3

(ACX3) and SOS3-INTERACTING PROTEIN 4 (SIP4) homologs in barley were suppressed to comparable levels between the genotypes upon salt treatment, two members of the GLYCOSYL HYDROLASE (GH) family 32 were shown to have their transcripts (HORVU7Hr1G001070.6, HORVU7Hr1G001070.19) maintained at higher levels in general for all root-zones when compared Clipper to Sahara. GH (aka. glycoside hydrolases or glycosidases) assist in the hydrolysis of glycosidic bonds in complex sugars or glucosides (such as indole-3-acetic acid-glucoside, salicylic glucoside, pyridoxine glucoside, flavone glucoside), which high concentration have shown to be strongly correlated to different abiotic stress responses in rice (Chern et al., 2005; Markham et al., 1998; Morino et al., 2005; Suzuki et al., 1986b; Suzuki et al., 1986a). Furthermore, transcripts encoded for a barley homolog (HORVU6Hr1G088460.1) of ASCORBATE PEROXIDASE 1 (APX1), which is a central component known for scavenging reactive oxygen species (ROS) in plant cells (Davletova et al., 2005), were also found to be co-regulated in this cluster. Intriguingly, transcript abundance of *APX1* was strongly induced Clipper Z2, but mostly suppressed in all root zones of Sahara (Supplementary Data Set 8 and 9: sheet 'sky-blue').

The subnetwork consisting of modules C, D, E, and F comprises members with in general stronger salinity-induced abundance for all root-zones in Sahara than in Clipper. **Module C** harboured 66 DEG and agmatine, which is a precursor of putrescine used for the production of 1,3-diaminopropane appeared only upon salt stress (Erdei et al., 1990), as the only DAM in this cluster. GO analysis suggested the biological processes most relevant to this cluster are toxin catabolism, raffinose biosynthesis, and glycine betaine biosynthesis (Fig. 7C). Barley homologs of two components (HORVU1Hr1G078350.1, HORVU2Hr1G070680.1) involved in the biosynthesis of glycine betaine via choline, namely PHOSPHOETHANOLAMINE METHYLTRANSFERASE1 (PEAMT) and ALDEHYDE DEHYDROGENASE 10A8 (ADH10A8), were found to be co-regulated in this cluster (McNeil et al., 2001; Missihoun et al., 2015). Glycine betaine is a type of known protectants *in vitro* or *in vivo* for mitigating the deleterious effect of salt stress in different plant species (Hasanuzzaman et al., 2014; Tian et al., 2017; Yildirim et al., 2015). Besides, two additional transcripts (HORVU1Hr1G060810.1, HORVU4Hr1G071300.12) encoding the barley homologs of GIBBERELLIN INSENSITIVE DWARF1C (GID1C) and ABERRANT GROWTH AND DEATH 2 (AGD2) were also identified in this co-expression cluster. GID1C and AGD2 were shown to be involved in the activation of gibberellin signalling by lifting the DELLA repressor activity (Ariizumi et al., 2008), and the induction of spontaneous cell death or suppression of callose deposition in plant

species (Rate and Greenberg, 2001), respectively (Supplementary Data Set 8 and 9: sheet 'orange-red'). **Module D** comprised of 39 DEG and significantly enriched in hemicellulose metabolism, sulphur metabolism, and transition metal ion homeostasis (Fig. 7D). Five transcripts (HORVU3Hr1G016850.1, HORVU5Hr1G048030.1, HORVU5Hr1G114540.1, HORVU4Hr1G089670.1, HORVU3Hr1G091400.1) encoded for barley homologs of XYLOGLUCAN ENDOTRANSGLUCOSYLASE/HYDROLASE 20 (XTH20), ESKIMO 1 (ESK1), PECTIN ACETYESTERASE 7 (PAE7), MUCILAGE-RELATED10 (MUCI10), and PLANT GLYCOGENIN-LIKE STARCH INITIATION PROTEIN 1 (PGSIP1), which were known to involve in organisation of different hemicelluloses in *A.thaliana* such as xyloglucan crosslink-formation, xylan backbone acetylation, pectin acetylation, glucomannan galactosylation, and galacturonic acid substitution of xylan, respectively (Zhong et al., 2018; Voiniciuc et al., 2015; Philippe et al., 2017; Urbanowicz et al., 2014; Miedes et al., 2013). While the abundance of *PGSIP1* were was similar for both Z2 and Z3 between the two genotypes, transcripts of *XTH20*, *ESK1*, and *PAE7* homologs reached higher abundance levels after the salt treatment in Z2 of Clipper, and in Z1, Z3 of Sahara. In contrast, abundance of *MUCI10* in all three root-zones were higher when compared Sahara to Clipper (Supplementary Data Set 8 and 9: sheet 'sienna'). **Module E** harboured 105 DEG ,and based on GO analysis indicated the most relevant biological processes in this cluster were systemic acquired resistance, regulation of endopeptidase, and response to ROS (Fig. 7E). Under the category of the acquired resistance, sequences of two transcripts (HORVU2Hr1G102050.1, HORVU2Hr1G102100.1) were found to be homologous to the *DEFECTIVE IN INDUCED RESISTANCE 1* (DIR1) (E-value = 5.00E-13; 7.00E-27) and one transcript (HORVU4Hr1G087860.1) was well-matched with its *AZELAIC ACID INDUCED 1* (AZI1) homolog in dicots (E-value = 4.00E-25). Intriguingly, both of these defence proteins were known to possess lipid binding and transfer abilities and overexpression of AZI1 was proven to increase salt tolerance of *A. thaliana* (Yu et al., 2013; Guelette et al., 2012). In addition, two transcripts (HORVU3Hr1G113120.1, HORVU5Hr1G018720.1) encoding for homologs of PATHOGENESIS-RELATED 4 (PR-4) (E-value = 2.00E-74) and RELATED TO AP2 11 (RAP2.11) (E-value = 7.00E-21) were co-regulated with members of this cluster. While transcript level of PR-4 was known to increase in response to ethylene and salt (Catinot et al., 2015; Kim et al., 2014), RAP2.11 expression was suggested to be positively feedback regulated by ethylene and ROS (Kim et al., 2012), which are commonly found in plant cells upon salinity stress (Supplementary Data Set 8 and 9: sheet 'plum'). **Module F** grouped 38 DEG and GO overrepresentation analysis suggested the metabolism of folic acid, tetrahydrofolate, and

pteridine were significantly upregulated in this cluster (Fig. 7F). Within this module, two transcripts (HORVU5Hr1G074900.1, HORVU5Hr1G074900.2) highly homologous to SARCOSINE OXIDASE (SOX) were also found to be induced to a much higher level of abundance in all root-zones of Sahara than in Clipper after salt. But unlike its homologs in *Corynebacterium* that catalyse the oxidation of sarcosine (Chlumsky et al., 1995), a non-protein amino acid known as pipecolate was determined as the endogenous substrate of SOX in plants (Goyer et al., 2004). Pipecolic acid was proven to be an endogenous mediator that orchestrates defence amplification, positive regulation of salicylic acid biosynthesis, and establishment of systemic acquired resistance In *A. thaliana* (Návarová et al., 2012). Oxidation of pipecolic acid mediated by the higher abundance of SOX in Sahara after salt could therefore imply a stronger suppression of such orchestration upon the local salinity impact (Supplementary Data Set 8 and 9: sheet 'saddle-brown').

In response to salinity stress, **Module H** was the only co-expression cluster with members highly up-regulated at Z1 and, for most cases, magnitudes of changes were higher in Sahara than Clipper. This cluster comprised 29 DEG and GO analysis revealed the most relevant biological processes were sterol biosynthesis and cell division (Fig. 7H). Among them, we found a transcript (HORVU2Hr1G011720.3) highly homologous to sequence of CYTOCHROME P450 51A2 (CYP51A2) in *A. thaliana* (E-value: 3.00E-172) with higher abundance only in Sahara Z1 in response to salinity stress. CYP51A2 is an upstream enzyme involved in the biosynthesis of brassinosteroids and modulation of membrane steroid contents, of which the membrane integrity maintained was proven to correlate to the restriction of ROS- and ethylene-mediated premature cell death (Kim et al., 2005; Kim et al., 2010). Further, three transcripts (HORVU2Hr1G073480.1, HORVU2Hr1G041950.1, HORVU6Hr1G071120.2) were homologs of CELL DIVISION CONTROL 2 (CDC2), CYCLIN P4;1 (CYCP4;1), and INDOLE-3-BUTYRIC ACID RESPONSE 5 (IBR5) and mostly up-regulated in Z1 of both genotypes upon salt, but with CDC2 and CYCP4;1 reaching higher abundance levels in Clipper, and IBR5 higher in Sahara, respectively. While IBR5 was proven to negatively regulate MAP kinase activity that control expression of cyclins in cell cycle (Johnson et al., 2015; Lee et al., 2009), CYCP4;1 and CDC2 are positive modulators of cell cycle progression and control of cell division (Torres Acosta et al., 2004; Zhao et al., 2012). On the whole, this suggests cell differentiation and division were highly constrained by salt in Z1 of Sahara, not in Clipper (Supplementary Data Set 8 and 9: sheet 'pale turquoise').

Lastly, **Module M** built up from members with abundance being predominantly induced at Clipper Z2, but substantially repressed at Z3 of both genotypes by salt. This module consists of 94 DEG that are significantly enriched in biological processes such as lipid localization, cell wall loosening, and receptor recycling (Fig. 7M). In this cluster, an exact match of UDP-D-GLUCURONATE 4-EPIMERASE 1 (GAE) known to be involved in pectin biosynthesis was also found at the top of the kME-ranked list (HORVU6Hr1G084390.1) (Gu and Bar-Peled, 2004), implying a potential role for maintaining barley root cell wall integrity played by members of this modules. Further, similar to the lipid-transporting AZI1 and DIR1 found in module E, sequences of six transcripts (HORVU7Hr1G109140.1, HORVU0Hr1G031750.1, HORVU0Hr1G025270.1, HORVU0Hr1G025250.2, HORVU2Hr1G097190.1, HORVU2Hr1G029480.1) were found to be highly homologous to members of the lipid transfer protein-related hybrid proline-rich protein (LTP-HyPRP) family, which is mostly bifunctional by exhibiting lipid-transporting and proteolytic activities (Pitzschke et al., 2014; Zhang and Schläppi, 2007). One of the most well-studied members of LTP-HyPRP is EARLY ARABIDOPSIS ALUMINIUM INDUCED 1 (EARLI1), which was shown to protect plant cells from freeze-induced damages and could improve root elongation under salt stress upon overexpressing *EARLI1* in *A. thaliana* (Xu et al., 2011; Zhang and Schläppi, 2007). Notably, a barley homolog (HORVU3Hr1G007280.2) encoded for another key enzyme involved in brassinosteroid biosynthesis known as STEROL 1 (STE1) was also found to be co-regulated in this cluster (Gachotte et al., 1995) (Supplementary Data Set 8 and 9: sheet 'pink').

Distinctive Phases of Salinity Responses Observed in Clipper and Sahara

As defined by (Julkowska and Testerink, 2015), responses of plant cells during the exposure to salinity stress can be categorized into four main phases, namely early signalling (ES) phase, quiescent (Q) phase, recovery (R) phase, and recovery extent (RE) phase. Responses induced at the ES phase, such as the salt overly sensitive (SOS) pathway (Shi, 2002) and aquaporin internalization (Prak et al., 2008), can be triggered and completed within seconds or mostly hours upon exposure to salt stress (Julkowska and Testerink, 2015). In this study, root zones of the two barley genotypes were presumably in stage of Q, R, or RE phase after three days of growth on media enriched with salt. Notably, in line with the striking growth differences observed amongst plant organs and between main and lateral roots in response to salt (Julkowska et al., 2014), our global co-expression correlation study reveals that salinity

impacts the two barley genotypes remarkably differently in terms of the phase of responses reached by their individual root zones. Implications from the molecular and hormonal clues of the study are summarized in Supplemental Table 2 (STable2) and discussed below.

Upon exposure to salt stress, inhibition of cell cycle progression restricted the cell division and differentiation processes in Sahara Z1 (STable2: Z1, Sahara). As substantial repression of the reactive oxygen species (ROS)-scavenging mechanisms in combination with the ethylene-mediated ROS accumulation were detected in this root zone, cells in Sahara Z1 were likely retained at Q phase and not RE phase in response to the salt treatment. Notably, the ROS-related activities in the apoplast mediate cell wall stiffening through crosslinking of glycoproteins and phenolic compounds, which are known to be the milestone events detected only at the Q phase upon salt stress (Tenhaken, 2014). By contrast, divisions of cells in Clipper Z1 were maintained and the corresponding biological processes for supporting rapid cell expansion, such as cellulose biosynthesis and cell wall loosening, were observed in Clipper Z2 (STable2: Z1, Clipper; Z2, Clipper). Although the positive modulation of cell divisions could indicate Clipper Z1 was in the stage subsequent to the Q phase (i.e. either R or RE phase), the significant upsurge of biosynthetic enzymes involved in brassinosteroid biosynthesis and initiation of the ROS-scavenging mechanism suggest Clipper Z2 was in R phase, and yet to be in RE phase. There are insufficient hormonal clues to help define the phase of responses for Clipper Z3 (STable2: Z3, Clipper). For Sahara Z2 and Z3, salt stress induced the expression of *C-REPEAT BINDING FACTOR 3* (*CBF3*) (STable2: Z2, Sahara; Z3, Sahara). In the presence of CBF, GIBBERELLIN 2-OXIDASE 7 (GA2OX7) specifically deactivates the bioactive C-20 gibberellins (GA) (Zhou et al., 2017). Assuming the amount of bioactive GA was minimal under the action of GA2OX7 in barley, GA signalling and thus its growth-promoting function was restricted in response to salinity stress, implying Sahara Z2 and Z3 was retained at Q phase after the three days of salt treatment.

Strengthening the conclusion drawn from the integrated pathway analysis, our global correlation study indicates that the Z2 of Clipper proceeded to R phase for restoration of its growth rate, while all root zones of Sahara remained at a prolonged Q phase in response to the extreme salinity conditions.

Furthermore, in addition to diverting the resources for maintenance of root growth, a range of known downstream salt tolerance mechanisms, such as polyamine transport and toxin

catabolism (Frommer et al., 1995; Roxas et al., 1997), were also activated in Z2 of Clipper in order to cope with the salinity stress (STable2: Z2, Clipper). Notably, the majority of the tolerance mechanisms triggered were different between Z2 and Z3 of Clipper, where biological processes including seed oil body formation, glucosinolate hydrolysis, and nicotianamine biosynthesis (Bonneau et al., 2016; Eriksson et al., 2002; Shimada et al., 2008) were either induced or maintained in Z3 of Clipper, but not in Z2 (STable2: Z3, Clipper). Only hydrolysis of glucosides (Markham et al., 1998) has widespread up-regulation in all root zones of Clipper (STable2: AZ, Clipper), suggesting the salt tolerance strategies adopted by this genotype are mostly root zone-dependent; a mechanism that can only be explicitly revealed by the spatial multi-omics approach described here.

In contrast, with only two salt-induced biological processes, membrane steroid modulation and inhibition of cell cycle progression, with members up-regulated or maintained at high abundance in Sahara Z1 (STable2: Z1, Sahara), seven out of seventeen processes in Sahara were shared among two root zones (STable2: asterisks). Members involved in the eight processes remained such as biosynthesis of glycine betaine, modulation of GA signalling, and LTP-mediated tolerance response in all root zones of Sahara were found to be induced or maintained at higher abundance than in Clipper (STable2: AZ, Sahara). This finding suggests the tolerance mechanisms triggered in Sahara were mostly root zone-independent. Such independence is also consistent with our viewpoint that all root zones of Sahara are in the same phase of the salinity response.

REFERENCES

Angelino, D., Dosz, E. B., Sun, J., Hoeflinger, J. L., Van Tassell, M. L., Chen, P., Harnly, J. M., Miller, M. J., and Jeffery, E. H. (2015). Myrosinase-dependent and -independent formation and control of isothiocyanate products of glucosinolate hydrolysis. Front Plant Sci *6*, 831.

Ariizumi, T., Murase, K., Sun, T. P., and Steber, C. M. (2008). Proteolysis-independent downregulation of DELLA repression in Arabidopsis by the gibberellin receptor GIBBERELLIN INSENSITIVE DWARF1. Plant Cell *20*, 2447-2459.

Bonneau, J., Baumann, U., Beasley, J., Li, Y., and Johnson, A. A. (2016). Identification and molecular characterization of the nicotianamine synthase gene family in bread wheat. Plant Biotechnol J *14*, 2228-2239.

Catinot, J., Huang, J. B., Huang, P. Y., Tseng, M. Y., Chen, Y. L., Gu, S. Y., Lo, W. S., Wang, L. C., Chen, Y. R., and Zimmerli, L. (2015). ETHYLENE RESPONSE FACTOR 96 positively regulates Arabidopsis resistance to necrotrophic pathogens by direct binding to GCC elements of jasmonate - and ethylene-responsive defence genes. Plant Cell Environ *38*, 2721-2734.

Chern, M., Fitzgerald, H. A., Canlas, P. E., Navarre, D. A., and Ronald, P. C. (2005). Overexpression of a rice NPR1 homolog leads to constitutive activation of defense response and hypersensitivity to light. Mol Plant Microbe Interact *18*, 511-520.

Chlumsky, L. J., Zhang, L., and Jorns, M. S. (1995). Sequence analysis of sarcosine oxidase and nearby genes reveals homologies with key enzymes of folate one-carbon metabolism. Journal of Biological Chemistry *270*, 18252-18259.

Cummins, I., Cole, D. J., and Edwards, R. (1999). A role for glutathione transferases functioning as glutathione peroxidases in resistance to multiple herbicides in black-grass. The Plant Journal *18*, 285-292.

Davletova, S., Rizhsky, L., Liang, H., Shengqiang, Z., Oliver, D. J., Coutu, J., Shulaev, V., Schlauch, K., and Mittler, R. (2005). Cytosolic ascorbate peroxidase 1 is a central component of the reactive oxygen gene network of Arabidopsis. Plant Cell *17*, 268-281.

Desprez, T., Juraniec, M., Crowell, E. F., Jouy, H., Pochylova, Z., Parcy, F., Höfte, H., Gonneau, M., and Vernhettes, S. (2007). Organization of cellulose synthase complexes involved in primary cell wall synthesis in Arabidopsis thaliana. Proceedings of the National Academy of Sciences *104*, 15572-15577.

Ellinger, D., and Kubigsteltig, I. I. (2010). Involvement of DAD1-like lipases in response to salt and osmotic stress in Arabidopsis thaliana. Plant Signal Behav *5*, 1269-1271.

Erdei, L., Trivedi, S., Takeda, K., and Matsumoto, H. (1990). Effects of osmotic and salt stresses on the accumulation of polyamines in leaf segments from wheat varieties differing in salt and drought tolerance. Journal of plant physiology *137*, 165-168.

Eriksson, S., Andréasson, E., Ekbom, B., Granér, G., Pontoppidan, B., Taipalensuu, J., Zhang, J., Rask, L., and Meijer, J. (2002). Complex formation of myrosinase isoenzymes in oilseed rape seeds are dependent on the presence of myrosinase-binding proteins. Plant Physiol *129*, 1592-1599.

Frommer, W. B., Hummel, S., Unseld, M., and Ninnemann, O. (1995). Seed and vascular expression of a high-affinity transporter for cationic amino acids in Arabidopsis. Proceedings of the National Academy of Sciences *92*, 12036-12040.

Fujioka, S., Li, J., Choi, Y. H., Seto, H., and Takatsuto…, S. (1997). The Arabidopsis deetiolated2 mutant is blocked early in brassinosteroid biosynthesis. The Plant …

Gachotte, D., Meens, R., and Benveniste, P. (1995). An Arabidopsis mutant deficient in sterol biosynthesis: heterologous complementation by ERG 3 encoding a Δ7-sterol-C-5-desaturase from yeast. The Plant Journal *8*, 407-416.

Goyer, A., Johnson, T. L., Olsen, L. J., Collakova, E., Shachar-Hill, Y., Rhodes, D., and Hanson, A. D. (2004). Characterization and metabolic function of a peroxisomal sarcosine and pipecolate oxidase from Arabidopsis. J Biol Chem *279*, 16947-16953.

Gu, X., and Bar-Peled, M. (2004). The biosynthesis of UDP-galacturonic acid in plants. Functional cloning and characterization of Arabidopsis UDP-D-glucuronic acid 4-epimerase. Plant Physiol *136*, 4256-4264.

Guelette, B. S., Benning, U. F., and Hoffmann-Benning, S. (2012). Identification of lipids and lipid-binding proteins in phloem exudates from Arabidopsis thaliana. Journal of experimental botany *63*, 3603-3616.

Han, Y., Chen, Y., Yin, S., Zhang, M., and Wang, W. (2015). Over-expression of TaEXPB23, a wheat expansin gene, improves oxidative stress tolerance in transgenic tobacco plants. J Plant Physiol *173*, 62-71.

Hasanuzzaman, M., Alam, M. M., Rahman, A., Hasanuzzaman, M., Nahar, K., and Fujita, M. (2014). Exogenous proline and glycine betaine mediated upregulation of antioxidant defense and glyoxalase systems provides better protection against salt-induced oxidative stress in two rice (Oryza sativa L.) varieties. Biomed Res Int *2014*, 757219.

Johnson, K. L., Ramm, S., Kappel, C., Ward, S., Leyser, O., Sakamoto, T., Kurata, T., Bevan, M. W., and Lenhard, M. (2015). The Tinkerbell (Tink) Mutation Identifies the Dual-Specificity MAPK Phosphatase INDOLE-3-BUTYRIC ACID-RESPONSE5 (IBR5) as a Novel Regulator of Organ Size in Arabidopsis. PLoS One *10*, e0131103.

Julkowska, M. M., Hoefsloot, H. C. J., Mol, S., Feron, R., de Boer, G.-J., Haring, M. A., and Testerink, C. (2014). Capturing Arabidopsis Root Architecture Dynamics with ROOT-FIT Reveals Diversity in Responses to Salinity. PLANT PHYSIOLOGY *166*, 1387-1402.

Julkowska, M. M., and Testerink, C. (2015). Tuning plant signaling and growth to survive salt. Trends in Plant Science *20*, 586-594.

Kampranis, S. C., Damianova, R., Atallah, M., Toby, G., Kondi, G., Tsichlis, P. N., and Makris, A. M. (2000). A novel plant glutathione S-transferase/peroxidase suppresses Bax lethality in yeast. J Biol Chem *275*, 29207-29216.

Kim, E. Y., Seo, Y. S., and Kim, W. T. (2011). AtDSEL, an Arabidopsis cytosolic DAD1-like acylhydrolase, is involved in negative regulation of storage oil mobilization during seedling establishment. J Plant Physiol *168*, 1705-1709.

Kim, H. B., Lee, H., Oh, C. J., Lee, H. Y., Eum, H. L., Kim, H. S., Hong, Y. P., Lee, Y., Choe, S., An, C. S., and Choi, S. B. (2010). Postembryonic seedling lethality in the sterol-deficient Arabidopsis cyp51A2 mutant is partially mediated by the composite action of ethylene and reactive oxygen species. Plant Physiol *152*, 192-205.

Kim, H. B., Schaller, H., Goh, C. H., Kwon, M., Choe, S., An, C. S., Durst, F., Feldmann, K. A., and Feyereisen, R. (2005). Arabidopsis cyp51 mutant shows postembryonic seedling lethality associated with lack of membrane integrity. Plant Physiol *138*, 2033-2047.

Kim, M. J., Ruzicka, D., Shin, R., and Schachtman, D. P. (2012). The Arabidopsis AP2/ERF transcription factor RAP2.11 modulates plant response to low-potassium conditions. Mol Plant *5*, 1042-1057.

Kim, S. A., Kwak, J., Jae, S.-K., Wang, M.-H., and Nam, H. (2001). Overexpression of the AtGluR2 Gene Encoding anArabidopsis Homolog of Mammalian Glutamate Receptors Impairs CalciumUtilization and Sensitivity to Ionic Stress in TransgenicPlants. Plant and Cell Physiology *42*, 74-84.

Kim, Y. J., Lee, H. J., Jang, M. G., Kwon, W. S., Kim, S. Y., and Yang, D. C. (2014). Cloning and characterization of pathogenesis-related protein 4 gene from Panax ginseng. Russian Journal of Plant Physiology *61*, 664-671.

Lee, J. S., Wang, S., Sritubtim, S., Chen, J.-G., and Ellis, B. E. (2009). Arabidopsis mitogen-activated protein kinase MPK12 interacts with the MAPK phosphatase IBR5 and regulates auxin signaling. The Plant Journal *57*, 975-985.

Lee, Y., Choi, D., and Kende, H. (2001). Expansins: ever-expanding numbers and functions. Current opinion in plant biology *4*, 527-532.

Lei, N., Yu, X., Li, S., Zeng, C., Zou, L., Liao, W., and Peng, M. (2017). Phylogeny and expression pattern analysis of TCP transcription factors in cassava seedlings exposed to cold and/or drought stress. Sci Rep *7*, 10016.

Markham, K. R., Tanner, G. J., Caasi-Lit, M., Whitecross, M. I., Nayudu, M., and Mitchell, K. A. (1998). Possible protective role for 3′, 4′-dihydroxyflavones induced by enhanced UV-B in a UV-tolerant rice cultivar. Phytochemistry *49*, 1913-1919.

McNeil, S. D., Nuccio, M. L., Ziemak, M. J., and Hanson, A. D. (2001). Enhanced synthesis of choline and glycine betaine in transgenic tobacco plants that overexpress phosphoethanolamine N-methyltransferase. Proceedings of the National Academy of Sciences *98*, 10001-10005.

Miedes, E., Suslov, D., Vandenbussche, F., Kenobi, K., Ivakov, A., Van Der Straeten, D., Lorences, E. P., Mellerowicz, E. J., Verbelen, J. P., and Vissenberg, K. (2013). Xyloglucan endotransglucosylase/hydrolase (XTH) overexpression affects growth and cell wall mechanics in etiolated Arabidopsis hypocotyls. J Exp Bot *64*, 2481-2497.

Mishina, T. E., and Zeier, J. (2006). The Arabidopsis flavin-dependent monooxygenase FMO1 is an essential component of biologically induced systemic acquired resistance. Plant Physiol *141*, 1666-1675.

Missihoun, T. D., Willée, E., Guegan, J. P., Berardocco, S., Shafiq, M. R., Bouchereau, A., and Bartels, D. (2015). Overexpression of ALDH10A8 and ALDH10A9 Genes Provides Insight into Their Role in Glycine Betaine Synthesis and Affects Primary Metabolism in Arabidopsis thaliana. Plant Cell Physiol *56*, 1798-1807.

Morino, K., Matsuda, F., Miyazawa, H., Sukegawa, A., Miyagawa, H., and Wakasa, K. (2005). Metabolic profiling of tryptophan-overproducing rice calli that express a feedback-insensitive alpha subunit of anthranilate synthase. Plant Cell Physiol *46*, 514-521.

Návarová, H., Bernsdorff, F., Döring, A. C., and Zeier, J. (2012). Pipecolic acid, an endogenous mediator of defense amplification and priming, is a critical regulator of inducible plant immunity. Plant Cell *24*, 5123-5141.

Philippe, F., Pelloux, J., and Rayon, C. (2017). Plant pectin acetylesterase structure and function: new insights from bioinformatic analysis. BMC Genomics *18*, 456.

Pitzschke, A., Datta, S., and Persak, H. (2014). Salt stress in Arabidopsis: lipid transfer protein AZI1 and its control by mitogen-activated protein kinase MPK3. Mol Plant *7*, 722-738.

Prak, S., Hem, S., Boudet, J., Viennois, G., Sommerer, N., Rossignol, M., Maurel, C., and Santoni, V. (2008). Multiple phosphorylations in the C-terminal tail of plant plasma membrane aquaporins: role in subcellular trafficking of AtPIP2;1 in response to salt stress. Mol Cell Proteomics *7*, 1019-1030.

Rate, D. N., and Greenberg, J. T. (2001). The Arabidopsis aberrant growth and death2 mutant shows resistance to Pseudomonas syringae and reveals a role for NPR1 in suppressing hypersensitive cell death. The Plant Journal *27*, 203-211.

Roxas, V. P., Smith Jr, R. K., Allen, E. R., and Allen, R. D. (1997). Overexpression of glutathione S-transferase/glutathioneperoxidase enhances the growth of transgenic tobacco seedlings during stress. Nature biotechnology *15*, 988.

Ruduś, I., Terai, H., Shimizu, T., Kojima, H., Hattori, K., Nishimori, Y., Tsukagoshi, H., Kamiya, Y., Seo, M., Nakamura, K., Kępczyński, J., and Ishiguro, S. (2014). Wound-induced expression of DEFECTIVE IN ANTHER DEHISCENCE1 and DAD1-like lipase genes is mediated by both CORONATINE INSENSITIVE1-dependent and independent pathways in Arabidopsis thaliana. Plant Cell Rep *33*, 849-860.

Saha, J., Brauer, E. K., Sengupta, A., Popescu, S. C., Gupta, K., and Gupta, B. (2015). Polyamines as redox homeostasis regulators during salt stress in plants. Frontiers in Environmental Science *3*, 2694.

Shani, Z., Dekel, M., Tsabary, G., and Shoseyov, O. (1997). Cloning and characterization of elongation specific endo-1, 4-β-glucanase (cel1) from Arabidopsis thaliana. Plant molecular biology *34*, 837-842.

Shi, H. (2002). The Putative Plasma Membrane Na+/H+ Antiporter SOS1 Controls Long-Distance Na+ Transport in Plants. THE PLANT CELL ONLINE *14*, 465-477.

Shimada, T. L., Shimada, T., Takahashi, H., Fukao, Y., and Hara-Nishimura, I. (2008). A novel role for oleosins in freezing tolerance of oilseeds in Arabidopsis thaliana. Plant J *55*, 798-809.

Shu, S., Yuan, Y., Chen, J., Sun, J., Zhang, W., Tang, Y., Zhong, M., and Guo, S. (2015). The role of putrescine in the regulation of proteins and fatty acids of thylakoid membranes under salt stress. Sci Rep *5*, 14390.

Suzuki, Y., Inada, Y., and Uchida, K. (1986a). β-Glucosylpyridoxines in germinating seeds cultured in the presence of pyridoxine. Phytochemistry *25*, 2049-2051.

Suzuki, Y., Ishii, H., Suga, K., and Uchida, K. (1986b). Formation of β-glucosylpyridoxines in soybean and rice callus. Phytochemistry *25*, 1331-1332.

Tenhaken, R. (2014). Cell wall remodeling under abiotic stress. Front Plant Sci *5*, 771.

Thompson, J. E., and Fry, S. C. (2001). Restructuring of wall-bound xyloglucan by transglycosylation in living plant cells. The Plant Journal *26*, 23-34.

Tian, F., Wang, W., Liang, C., Wang, X., Wang, G., and Wang, W. (2017). Overaccumulation of glycine betaine makes the function of the thylakoid membrane better in wheat under salt stress. The Crop Journal *5*, 73-82.

Torres Acosta, J. A., de Almeida Engler, J., Raes, J., Magyar, Z., De Groodt, R., Inzé, D., and De Veylder, L. (2004). Molecular characterization of Arabidopsis PHO80-like proteins, a novel class of CDKA;1-interacting cyclins. Cell Mol Life Sci *61*, 1485-1497.

Urbanowicz, B. R., Peña, M. J., Moniz, H. A., Moremen, K. W., and York, W. S. (2014). Two Arabidopsis proteins synthesize acetylated xylan in vitro. Plant J *80*, 197-206.

Voiniciuc, C., Schmidt, M. H., Berger, A., Yang, B., Ebert, B., Scheller, H. V., North, H. M., Usadel, B., and Günl, M. (2015). MUCILAGE-RELATED10 Produces Galactoglucomannan That Maintains Pectin and Cellulose Architecture in Arabidopsis Seed Mucilage. Plant Physiol *169*, 403-420.

Wang, X., Gao, J., Zhu, Z., Dong, X., Wang, X., Ren, G., Zhou, X., and Kuai, B. (2015). TCP transcription factors are critical for the coordinated regulation of isochorismate synthase 1 expression in Arabidopsis thaliana. Plant J *82*, 151-162.

Xu, D., Huang, X., Xu, Z. Q., and Schläppi, M. (2011). The HyPRP gene EARLI1 has an auxiliary role for germinability and early seedling development under low temperature and salt stress conditions in Arabidopsis thaliana. Planta *234*, 565-577.

Yildirim, E., Ekinci, M., Turan, M., Dursun, A., Kul, R., and Parlakova, F. (2015). Roles of glycine betaine in mitigating deleterious effect of salt stress on lettuce (L.). Archives of Agronomy and Soil Science *61*, 1673-1689.

Yu, K., Soares, J. M., Mandal, M. K., Wang, C., Chanda, B., Gifford, A. N., Fowler, J. S., Navarre, D., Kachroo, A., and Kachroo, P. (2013). A feedback regulatory loop between G3P and lipid transfer proteins DIR1 and AZI1 mediates azelaic-acid-induced systemic immunity. Cell Rep *3*, 1266-1278.

Zhang, Y., and Schläppi, M. (2007). Cold responsive EARLI1 type HyPRPs improve freezing survival of yeast cells and form higher order complexes in plants. Planta *227*, 233-243.

Zhao, X., Harashima, H., Dissmeyer, N., Pusch, S., Weimer, A. K., Bramsiepe, J., Bouyer, D., Rademacher, S., Nowack, M. K., Novak, B., Sprunck, S., and Schnittger, A. (2012). A general G1/S-phase cell-cycle control module in the flowering plant Arabidopsis thaliana. PLoS Genet *8*, e1002847.

Zhong, R., Cui, D., Phillips, D. R., and Ye, Z. H. (2018). A Novel Rice Xylosyltransferase Catalyzes the Addition of 2-O-Xylosyl Side Chains onto the Xylan Backbone. Plant Cell Physiol *59*, 554-565.

Zhou, M., Chen, H., Wei, D., Ma, H., and Lin, J. (2017). Arabidopsis CBF3 and DELLAs positively regulate each other in response to low temperature. Sci Rep *7*, 39819.

Supplemental Note 3

Functional Annotation of the New Barley Reference Genome

To further enrich the functional annotations of the mapping base for RNA-seq, the latest version of the new barley reference genome sequences (cv. Morex v2) and the genome structural annotation files were obtained from IPK Barley server of the International Barley Sequencing Consortium (IBSC) (Mascher et al., 2017). The total population of coding sequences of the genome was extracted by the gffread utility of Cufflinks (Trapnell et al., 2012) and refined using the degapseq script of EMBOSS 6.6.0.0 (Rice et al., 2000). The latest version of Basic Local Alignment Search Tool (BLAST) was obtained from the FTP server of the National Center for Biotechnology Information (NCBI) (Altschul et al., 1990), and a local BLAST pipeline was constructed in eight NeCTAR Research Cloud instances in Ubuntu 16.04 LTS (Xenial) environment (Li et al., 2018). The total population of translated coding sequences of the barley genome were BLASTx searched against three protein sequence databases, i.e. TAIR10 (Lamesch et al., 2012), UniProtKB/Swiss-Prot (The UniProt Consortium, 2017), RAP-DB (Sakai et al., 2013), and two ontology databases i.e. Gene Ontology (GO) (Ashburner et al., 2000) and KEGG Ontology (KO) (Kanehisa and Goto, 2000). The latest version of InterProScan-5 and Panther models 10.0 were obtained from the FTP server of the European Bioinformatics Institute (EMBL-EBI) and the getorf script of EMBOSS was applied to make InterProScan-5 to be compatible to nucleotide inputs. Scanning of InterPro protein domains databases was performed according to the user manual (Jones et al., 2014). Only the top hits of each coding sequence with the lowest e-values were listed in the functional annotation list and considered for biological interpretation.

Read Processing, and Mapping

Paired-end libraries of raw reads from the RNA-seq were verified and converted using FASTQ Groomer (Blankenberg et al., 2010) and sequence quality was validated using FastQC (Andrews). Based on the outcomes of the read quality assessment, threshold was defined (q=20; minimum read length: 24; Illumina TruSeq Adaptor primers removed; singletons discarded) and Trimmomatic was applied to trim reads for quality (Bolger et al., 2014). Mapping or paired-read alignment was performed via HISAT2 (Kim et al., 2015) and the sorted BAM files were

subjected to HTSeq code (Anders et al., 2015) for generation of the counting matrix using the genome structural annotation available from IBSC (Mascher et al., 2017).

DEG Determination and Enrichment Analysis of Gene Ontologies

To prepare for DEG determination, we filtered the lowly expressed genes from the matrix were filtered based on a minimum CPM threshold of 11.5 present in at least four samples, which corresponds to an average read count of 10-15 across the 192 libraries, to minimise the multiple testing burden when estimating false discovery rates (Robinson et al., 2010). TMM normalization was applied to the transformed CPM matrix to eliminate composition biases between libraries (Robinson and Oshlack, 2010). Multidimensional scaling of the TMM-normalized matrix explicitly revealed one biological replicate of Clipper control at Z3 as an outlier and was therefore excluded from all subsequent analyses. Variation of library sizes, sample-specific quality weighting, and mean-variance dependence of the data matrix were addressed by the voom transformation workflow available in limma package (v.3.7) (Ritchie et al., 2015). Detailed procedures for estimating group mean and gene-wise variances, as well as fitting of basic and interaction GLM to test for differential expression were detailed in (Smyth et al., 2002). Notably, as discussed by (Zhang and Cao, 2009), assumptions required for fold-change filtering and *t*-statistic adopted in DEG determination were contradictory, therefore only the *t*-statistic-based adjusted *p* value was applied as a cutoff in this study.

For enrichment analysis of GO, BiNGO was applied to determine the overrepresented GO terms in each DEG list focusing only on the GO Biological Processes category (Maere et al., 2005). Unless otherwise specified, the analyses were performed using the hypergeometric test with the whole barley annotation as a reference set and Benjamini-Hochberg FDR correction with *q* value cutoff at 0.05. Each enrichment list was summarized by REVIGO with small (0.5) allowed similarity (Supek et al., 2011) and enrichment networks resulted were visualized in Cytoscape (v.3.4.0) (Shannon, 2003).

DAM Determination and Metabolite Set Enrichment Analysis

Data matrices corresponding to each type of primary metabolomes and phenylpropanoids were standardized by sample weights to achieve unit-conformity across different extraction and detection workflows. To reduce systemic bias during sample collection and impact of the large

feature (metabolite) values, log-transformed matrices were normalized by median across samples and mean-centred, respectively (van den Berg et al., 2006). Each normalized matrix was individually evaluated for unwanted variances by means of relative log adjustment - within group (RLAwg), principal component analysis (PCA), and hierarchical-clustering (HCR) (Xia and Wishart, 2011), which unambiguously indicated one out of four of the biological replicates in the primary metabolome detection as an outlier which was therefore excluded from all subsequent analyses. Potential batch effects attributed to sample degradation and/or instrumentation platform differences were evaluated and adjusted using the RUV-R method (Livera et al., 2015). For determination of DAM, a limma-based linear modelling algorithm fitted with moderate statistics (simple Bayesian model) developed by (Livera and Bowne, 2014) was adopted to construct the basic and interaction GLM contrasts required for determination of DAM. MBROLE (v.2.0) with use of the full database as reference set, but selected only the functional roles that are non-ambiguous and can be found in the *Plantae*, were utilized to detect the enrichment of metabolite sets of each list of DAM (López-Ibáñez et al., 2016).

Integrated Pathway Analysis

To integrate the omics datasets at the pathway level, coding sequences of DEGs identified from the differential analyses of the twelve transcriptomes upon salt treatment were translated and BLASTx searched against the *Arabidopsis* genome release (TAIR10, version: Jun 2016) and KEGG pathway repository (version: May 2017). Only matches with E-value < $1.00E^{-4}$ (or smallest possible E-value in the case of multiple hits for the same gene) against either or both databases were retained and corresponding K numbers in the KEGG repository were fetched for the subsequent integration step. For primary metabolites, the C numbers of DAMs detected in each LC/GC-MS-based quantification were determined by comparison of their chemical structures, formulae, molecular weights, and/or IUPAC nomenclatures between the reference standards used and the KEGG compound repository (May 2017). KEGG mapping of the K and C numbers acquired was performed against the pathway repository of *Arabidopsis thaliana*, which is the most comprehensive and representative pathway collection among all plant species within the KEGG database, following the procedures as stated previously (Aoki and Kanehisa, 2005). Generic outputs from the KEGG mapper (including: ath01100 Metabolic pathways, ath01110 Biosynthesis of secondary metabolites) were defined as outputs from the KEGG mapper common to any kind of inputs and were therefore excluded from the ranking process. Only pathways statistically enriched in terms of GO categories (as determined by BiNGO) and

of metabolite sets (as determined by MBROLE2) were ranked in descending order according to the number of significant DEG and DAM matches.

Correlation Network

Abundance matrices of the total population of DEG and DAM from each barley genotype were concatenated as individual inputs for the Weighted Correlation Network Analysis (WGCNA). Processing of the matrices and network comparisons were performed as described (Langfelder and Horvath, 2008). In brief, matrices were evaluated for missing value using the goodSamplesGenes function and any outliers were determined by hierarchical clustering. Scale-free topology and mean connectivity of each network were plotted against the soft thresholding power to derive the optimal adjacency or dissimilarity. Two coexpression correlation networks (also known as hierarchical clustering of transcript and metabolite abundance) specific to Clipper and Sahara were built based on dissimilarity-based topological overlap matrix (TOM). Modules of each network were defined by dynamicTreeCut and modules unique to each network were determined the matchModules function. Comparability of the two matrices was confirmed by verifying the correlation of ranked expression and ranked connectivity between the two datasets. Module preservation between the independent coexpression-correlation networks of Clipper (as 'reference' set) and Sahara (as 'test' set) were calculated by the 'modulePreservation' function of the WGCNA package v1.61, which outputted the 'Zsummary.pres' value for each module based on preservation-statistics and module quality-statistics (including quality, preservation, accuracy, reference separability, and test separability). $Z>10$ (including modules brown, turquoise, yellow, blue, greenyellow, and green), $5<Z<10$ (including black, purple, red, cyan, pink), and $Z<5$ (including magenta, tan, salmon) indicate high preservation, moderate preservation, and low preservation or modules with significant contrast, respectively. Modules with Z-score <10, excluding module 'tan', which was determined as noise, are defined as weakly preserved modules or modules with significant contrast between the two barley genotypes. Parallel plots for showing either positive or negative correlation of different abundance clusters (within 99^{th} percentile) were generated using the ggplot package of R software. The most representative trend or centroid of each module represented by purple solid lines was determined by k-mean clustering (distance method: Pearson) with optimal number of clusters calculated using the within-group sum of square method (Madsen and Browning, 2009). Module memberships (kME) of genes and

metabolites harboured among module or cluster unique to either network or significantly different to the other network were calculated by signedKME function of the WGCNA package.

REFERENCES

Altschul, S. F., Gish, W., Miller, W., Myers, E. W., and Lipman, D. J. (1990). Basic local alignment search tool. Journal of molecular biology *215*, 403-410.

Anders, S., Pyl, P. T., and Huber, W. (2015). HTSeq--a Python framework to work with high-throughput sequencing data. Bioinformatics *31*, 166-169.

Andrews, S. FastQC: a quality control tool for high throughput sequence data. Available online at: http://www.bioinformatics.babraham.ac.uk/projects/fastqc.

Aoki, K. F., and Kanehisa, M. (2005). Using the KEGG database resource. Current protocols in bioinformatics *11*, 1.12. 1-1.12. 54.

Ashburner, M., Ball, C. A., Blake, J. A., Botstein, D., Butler, H., Cherry, J. M., Davis, A. P., Dolinski, K., Dwight, S. S., and Eppig, J. T. (2000). Gene Ontology: tool for the unification of biology. Nature genetics *25*, 25.

Blankenberg, D., Gordon, A., Von Kuster, G., Coraor, N., Taylor, J., Nekrutenko, A., and Galaxy, T. (2010). Manipulation of FASTQ data with Galaxy. Bioinformatics *26*, 1783-1785.

Bolger, A. M., Lohse, M., and Usadel, B. (2014). Trimmomatic: a flexible trimmer for Illumina sequence data. Bioinformatics *30*, 2114-2120.

Jones, P., Binns, D., Chang, H. Y., Fraser, M., Li, W., McAnulla, C., McWilliam, H., Maslen, J., Mitchell, A., Nuka, G., Pesseat, S., Quinn, A. F., Sangrador-Vegas, A., Scheremetjew, M., Yong, S. Y., Lopez, R., and Hunter, S. (2014). InterProScan 5: genome-scale protein function classification. Bioinformatics *30*, 1236-1240.

Kanehisa, M., and Goto, S. (2000). KEGG: kyoto encyclopedia of genes and genomes. Nucleic acids research *28*, 27-30.

Kim, D., Langmead, B., and Salzberg, S. L. (2015). HISAT: a fast spliced aligner with low memory requirements. Nat Methods *12*, 357-360.

Lamesch, P., Berardini, T. Z., Li, D., Swarbreck, D., Wilks, C., Sasidharan, R., Muller, R., Dreher, K., Alexander, D. L., Garcia-Hernandez, M., Karthikeyan, A. S., Lee, C. H., Nelson, W. D., Ploetz, L., Singh, S., Wensel, A., and Huala, E. (2012). The Arabidopsis Information Resource (TAIR): improved gene annotation and new tools. Nucleic Acids Res *40*, D1202-10.

Langfelder, P., and Horvath, S. (2008). WGCNA: an R package for weighted correlation network analysis. BMC Bioinformatics *9*, 559.

Li, Z., Ranjan, R., O'Brien, L., Zhang, H., Ali Babar, M., Zomaya, A. Y., and Wang, L. (2018). On the Communication Variability Analysis of the NeCTAR Research Cloud System. IEEE Systems Journal *12*, 1506-1517.

Livera, A. M. D., and Bowne, J. B. (2014). Analysis of Metabolomics Data. Available online at: https://cran.r-project.org/web/packages/metabolomics/metabolomics.pdf.

Livera, A. M. D., Sysi-Aho, M., Jacob, L., Gagnon-Bartsch, J. A., Castillo, S., Simpson, J. A., and Speed, T. P. (2015). Statistical Methods for Handling Unwanted Variation in Metabolomics Data. Analytical Chemistry *87*, 3606-3615.

López-Ibáñez, J., Pazos, F., and Chagoyen, M. (2016). MBROLE 2.0-functional enrichment of chemical compounds. Nucleic Acids Res *44*, W201-4.

Madsen, B. E., and Browning, S. R. (2009). A groupwise association test for rare mutations using a weighted sum statistic. PLoS Genet *5*, e1000384.

Maere, S., Heymans, K., and Kuiper, M. (2005). BiNGO: a Cytoscape plugin to assess overrepresentation of gene ontology categories in biological networks. Bioinformatics *21*, 3448-3449.

Mascher, M., Gundlach, H., Himmelbach, A., Beier, S., Twardziok, S. O., Wicker, T., Radchuk, V., Dockter, C., Hedley, P. E., Russell, J., Bayer, M., Ramsay, L., Liu, H., Haberer, G., Zhang, X. Q., Zhang, Q., Barrero, R. A., Li, L., Taudien, S., Groth, M., Felder, M., Hastie, A., Šimková, H., Staňková, H., Vrána, J., Chan, S., Muñoz-Amatriaín, M., Ounit, R., Wanamaker, S., Bolser, D., Colmsee, C., Schmutzer, T., Aliyeva-Schnorr, L., Grasso, S., Tanskanen, J., Chailyan, A., Sampath, D., Heavens, D., Clissold, L., Cao, S., Chapman, B., Dai, F., Han, Y., Li, H., Li, X., Lin, C., McCooke, J. K., Tan, C., Wang, P., Wang, S., Yin, S., Zhou, G., Poland, J. A., Bellgard, M. I., Borisjuk, L., Houben, A., Doležel, J., Ayling, S., Lonardi, S., Kersey, P., Langridge, P., Muehlbauer, G. J., Clark, M. D., Caccamo, M., Schulman, A. H., Mayer, K. F. X., Platzer, M., Close, T. J., Scholz, U., Hansson, M., Zhang, G., Braumann, I., Spannagl, M., Li, C., Waugh, R., and Stein, N. (2017). A chromosome conformation capture ordered sequence of the barley genome. Nature *544*, 427-433.

Rice, P., Longden, I., and Bleasby, A. (2000). EMBOSS: the European molecular biology open software suite. Trends in genetics *16*, 276-277.

Ritchie, M. E., Phipson, B., Wu, D., Hu, Y., Law, C. W., Shi, W., and Smyth, G. K. (2015). limma powers differential expression analyses for RNA-sequencing and microarray studies. Nucleic Acids Res *43*, e47.

Robinson, M. D., McCarthy, D. J., and Smyth, G. K. (2010). edgeR: a Bioconductor package for differential expression analysis of digital gene expression data. Bioinformatics *26*, 139-140.
Robinson, M. D., and Oshlack, A. (2010). A scaling normalization method for differential expression analysis of RNA-seq data. Genome Biol *11*, R25.
Sakai, H., Lee, S. S., Tanaka, T., Numa, H., Kim, J., Kawahara, Y., Wakimoto, H., Yang, C. C., Iwamoto, M., Abe, T., Yamada, Y., Muto, A., Inokuchi, H., Ikemura, T., Matsumoto, T., Sasaki, T., and Itoh, T. (2013). Rice Annotation Project Database (RAP-DB): an integrative and interactive database for rice genomics. Plant Cell Physiol *54*, e6.
Shannon, P. (2003). Cytoscape: A Software Environment for Integrated Models of Biomolecular Interaction Networks. Genome Research *13*, 2498-2504.
Smyth, G. K., Ritchie, M., Thorne, N., Wettenhall, J., Shi, W., and Hu, Y. (2002). limma: Linear Models for Microarray and RNA-Seq Data User's Guide.
Supek, F., Bošnjak, M., Škunca, N., and Šmuc, T. (2011). REVIGO summarizes and visualizes long lists of gene ontology terms. PLoS One *6*, e21800.
The UniProt Consortium (2017). UniProt: the universal protein knowledgebase. Nucleic Acids Res *45*, D158-D169.
Trapnell, C., Roberts, A., Goff, L., Pertea, G., Kim, D., Kelley, D. R., Pimentel, H., Salzberg, S. L., Rinn, J. L., and Pachter, L. (2012). Differential gene and transcript expression analysis of RNA-seq experiments with TopHat and Cufflinks. Nat Protoc *7*, 562-578.
van den Berg, R. A., Hoefsloot, H. C., Westerhuis, J. A., Smilde, A. K., and van der Werf, M. J. (2006). Centering, scaling, and transformations: improving the biological information content of metabolomics data. BMC Genomics *7*, 142.
Xia, J., and Wishart, D. S. (2011). Web-based inference of biological patterns, functions and pathways from metabolomic data using MetaboAnalyst. Nature Protocols *6*, 743-760.
Zhang, S., and Cao, J. (2009). A close examination of double filtering with fold change and T test in microarray analysis. BMC Bioinformatics *10*, 402.

Supplemental Table 1. Quantitative Assessment of Module Preservation Between the Genotype-specific Correlation Networks.

Module	Size of Modules	Zsummary.pres
brown	381	26.0347534
turquoise	400	21.5008584
yellow	330	21.2736166
blue	400	18.3925979
grey	400	14.6007575
greenyellow	176	11.6411528
green	243	10.4537462
black	173	9.0217124
gold	100	8.6063239
purple	126	8.2068145
red	222	6.7381024
cyan	59	5.9966218
pink	136	5.6553828
magenta	184	2.9000761
tan	33	1.0179650
salmon	106	0.8221007

The grey module contains uncharacterized genes and the gold module contains random genes as determined in a permutation test with 30 permutations. Zsummary.pres represents the Z-score summary statistics of module preservation. In general, the higher the value of “Zsummary.pres”, the more preserved the module is between the datasets ($Z<5$ suggests low preservation, $5<Z<10$ indicates moderate preservation, and $Z>10$ indicates high preservation). Grey and gold modules contains uncharacterized and random genes respectively.

Supplemental Table 2. Summary of the global coexpression correlation analyses of the two barley genotypes under salinity.

	Clipper			Sahara		
	Biological Process	**Module**	**RMM**	**Biological Process**	**Module**	**RMM**
Z1	- positive modulation of cell division	H	*CYCP4;1, CDC2*	- ROS-scavenging mechanism (suppression) *	I	*APX1*
				- lipase-mediate JA biosynthesis *	G	*DALL1*
				- xyloglucan crosslink-formation *	D	*XTH20*
				- xylan backbone acetylation *	D	*ESK1*
				- pectin acetylation *	D	*PAE7*
				- membrane steroid modulation	H	*CYP51A2*
				- inhibition of cell cycle progression	H	*IBR5*
Z2	- cell elongation	A	*CEL1*	- cell wall-bound peroxidase *	J	*EXPB2*
	- calcium ion homeostasis	J	*GLR2.7*	- suppression of GA biosynthesis and signalling *	B	*CBF3*
	- polyamine transport	K	*AAT1*			
	- toxin catabolism	K	*GSTU18*			
	- cellulose biosynthesis	L	*CESA1, CESA3*			
	- cell wall loosening	L	*EXPA11, B4, A7*			
	- brassinosteroid biosynthesis	L	*DET2*			
		M	*STE1*			
	- regulation of SA biosynthesis	L	*TCP8, 15, 23*			
	- ROS-scavenging mechanism	I	*APX1*			
	- crosslinking of xyloglucan	D	*XTH20*			
	- xylan backbone acetylation	D	*ESK1*			
	- pectin acetylation	D	*PAE7*			
	- pectin biosynthesis	M	*GAE*			
	- lipid transport and proteolysis	M	*LTP-HyPRP*			
Z3	- cell wall organization	N	*XTH13*	- cell wall-bound peroxidase *	N	*EXPA2, A13, B2*
	- seed oil body formation	N	*DSEL, OLE1*	- suppression of GA biosynthesis and signalling *	B	*CBF3*
	- glucosinolate hydrolysis	B	*MBP1*			
	- nicotianamine biosynthesis	O	*NAS3, NAS4*	- lipase-mediated JA biosynthesis *	G	*DALL1*
				- ROS-scavenging mechanism (suppression) *	I	*APX1*
				- xyloglucan crosslink-formation *	D	*XTH20*
				- xylan backbone acetylation *	D	*ESK1*
				- pectin acetylation *	D	*PAE7*
AZ	- hydrolysis of glucosides	I	*GH*	- biosynthesis of glycine betaine	C	*PEAMT, ADH10A8*
				- modulation of GA signalling	C	*GID1C*
				- suppression of callose deposition	C	*AGD2*
				- glucomannan galactosylation	D	*MUCI10*
				- LTP-mediated defense/ salt tolerance response	E	*DIR1, AZI1*
				- salinity-/ ethylene-responsive	E	*PR-4*
				- ethylene-/ ROS-responsive	E	*RAP2.11*
				- suppression of defense amplification	F	*SOX*

Only biological processes with modular members being induced or remained at higher abundance after the salt treatment in different root zones of the two barley genotypes are listed. Asterisks indicate biological processes that shared between two root zones. AZ, all zones (including zone 1, 2, and 3); GA, gibberellin; JA, jasmonic acid; LTP, lipid transfer protein; RMM, representative modular member(s); ROS, reactive oxygen species; SA, salicylic acid; Z1, zone 1 (meristematic); Z2, zone 2 (elongation); Z3, zone 3 (maturation).